

Charged lepton flavor violating processes in the Grimus-Neufeld model

Vytautas Dūdėnas ^{a,1} Thomas Gajdosik ^a Uladzimir Khasianeovich ^b Wojciech Kotlarski ^c Dominik Stöckinger^b

^a*Institute of Theoretical Physics and Astronomy, Faculty of Physics, Vilnius University, 9 Saultėkio, LT-10222 Vilnius, Lithuania*

^b*Institut für Kern- und Teilchenphysik, TU Dresden, Zellescher Weg 19, 01069 Dresden, Germany*

^c*National Centre for Nuclear Research, Pasteura 7, 02-093 Warsaw, Poland*

E-mail: vytautasdudenas@inbox.lt, thomas.gajdosik@cern.ch,
uladzimir.khasianeovich@tu-dresden.de, wojciech.kotlarski@ncbj.gov.pl,
dominik.stoeckinger@tu-dresden.de

ABSTRACT: Charged Lepton Flavour Violating (cLFV) decays constrain the relationship between the neutrino and the scalar sectors of the Grimus-Neufeld model (GNM), an appealing minimal model of neutrino masses. It turns out, that in the scenario, where the seesaw scale is lower than the electroweak one, cLFV is completely defined by the new Yukawa interactions between the additional single heavy Majorana neutrino, the second Higgs doublet and the lepton doublets. Therefore, we derive a useful parameterization for the Yukawa couplings which reproduces by construction the correct PMNS matrix and the correct neutrino masses for both Normal and Inverted ordering at one-loop level. We embed this scenario in the FlexibleSUSY spectrum-generator generator to perform parameter scans. Focusing on the tiny seesaw scale, we show that current $\mu \rightarrow e\gamma$ limits provide significant constraints on the scalar sector, and we evaluate the impact of future cLFV τ -decay searches for the cases of discovery or non-discovery. The tiny seesaw scale makes the neutrino sector and the cLFV processes in the GNM similar to the scotogenic and the scoto-seesaw models, so we provide constraints for these models as well.

¹Corresponding author.

Contents

1	Introduction	1
2	The Grimus-Neufeld model	3
2.1	Scalar and Yukawa sectors	4
2.2	Rotations for neutrinos	5
2.3	Neutrino mass matrix	9
2.4	Vanishing $Y^{(2)}$	11
2.5	Reproducing neutrino masses and mixings	12
3	Charged Lepton Flavor Violating processes	12
3.1	Coefficients	13
3.2	Decay widths	15
4	Recap of important parameters	16
5	Phenomenological analysis	17
5.1	Discussion of the relative importance of different decay modes	17
5.2	Current and planned restrictions on $ \Lambda m_{H^\pm}^2$	18
5.3	Some processes are observed: restrictions on the $\omega_{22} - r$ plane	19
5.4	Nothing is observed: future absolute bounds on $ \Lambda m_{H^\pm}^2$	21
5.5	Interpretation of results: example of limits on λ_5 and relations to scoto-seesaw and scotogenic models	22
6	Conclusions	24
A	Parametrization for Yukawa couplings	25
B	Determining the minimal parameter space	27
C	Relations between Yukawa couplings of different parameter points	30
D	Numerical values for Yukawas on the $\omega_{22} - r$ plane	31

1 Introduction

Many years have passed since the discovery of neutrino oscillations [1–4], yet massive neutrinos are still not in the Standard model (SM). That is not surprising: it is extremely hard to either confirm or exclude all the possible mechanisms that generate neutrino masses due to their weak impact on the sectors that we can actually see in the experiments, see

e.g. studies of the low energy effects of the seesaw mechanisms in [5, 6]. However, having in mind the impressive precision of current Charged Lepton Flavour Violation (cLFV) experiments [7–10] some of the scenarios can actually lead to possible signatures and/or restrictions on the parameter spaces, and will become even more restricting in the future, given planned experiments [11–15]. Hence, it makes sense to look at the most constraining scenarios to narrow down the possible space of the neutrino mass mechanisms.

The simplest neutrino mass mechanisms can be put into three categories: inducing neutrino masses at tree-level (e.g. all types of seesaw [16–18]), generating them at loops (see e.g. [19–21]), and combining these mechanisms (e.g. [22, 23]). These mass mechanisms can be embedded into more exotic models, for example, the seesaw mechanism can arise from extra dimensions [24, 25], or radiative neutrino generation can be realized with composite Higgses [26, 27]. While virtually all scenarios can fit the current experimental constraints, it is far harder to claim the strictly excluded regions unambiguously, especially when one studies more general scenarios with an overwhelming number of free parameters (see e.g. [28]). A look at less general models, with more exposed and isolated effects on the cLFV from the neutrino sector, naturally provides a solution to this problem.

The scotogenic model [21] is probably the most popular one in this respect, partially due to a manageable amount of free parameters. With an imposed Z_2 symmetry, it has the scalar sector of the inert doublet model (IDM) [29]. The cLFV in the scotogenic model comes purely from the radiative contributions of heavy neutrinos and scalar dark matter candidates [30, 31]. Thus, the neutrino sector acts as a bridge between the dark scalar sector and cLFV.

There is an interesting variation, called the scoto-seesaw model [32, 33], with even fewer degrees of freedom introduced. In both models, scotogenic and scoto-seesaw, one obtains larger contributions to the cLFV for lower heavy neutrino masses. This potentially implies stronger restrictions on the scalar sector. We define a *tiny* seesaw scale to be lower than the electroweak scale (studied in e.g. [34–38]), to discriminate between the low seesaw scale that is sometimes considered to include the TeV scale (e.g. [39–41]). Then, in the tiny seesaw scale, the scotogenic and the scoto-seesaw models give essentially the same contribution to cLFV as we get in the Grimus-Neufeld model (GNM) [22] — a seesaw extended two-Higgs-doublet model (2HDM). This connection is caused by an approximate Z_2 symmetry in the Yukawa sector [42] (discussed in the next section), which makes the radiative neutrino mass generation in the GNM similar to the one in the scotogenic and scoto-seesaw models.

Global symmetries, such as Z_2 , are extremely useful for classifying the scenarios of beyond Standard model (BSM) physics. Yet they are not something fundamental. If one imposes a global symmetry only on one part of the Lagrangian, while breaking at some other part of it, at some loop order it eventually leads to breakage of the imposed symmetry in the sector of interest too. From one point of view, one might conclude that imposing a global symmetry is only consistent if it is done on the full Lagrangian. On the other hand, if one looks at global symmetries as something that just helps us to classify possible scenarios of BSM physics, there is no real need to insist on satisfying it exactly at all loop levels. For example, the CP-symmetric 2HDM potential might get CP-violating corrections from the quark sector, as discussed in [43]. There are many studies on CP-conserving 2HDM

potential, which nevertheless are meaningful and explore an important possible scenario of the scalar sector. This naturally leads to a question: what if some parameters in the Lagrangian are so small, that we can *almost* see the global symmetry? This generalizes the concept of the global symmetry of the Lagrangian by allowing small deviations from zero of the symmetry breaking terms. Following this logic, we will loosely define the approximate symmetry to be the case in which the Lagrangian parameters that explicitly break the global symmetry are not necessarily zero, but are very small (in our case, smaller than $O(10^{-7})$). The GNM satisfies this requirement in the tiny seesaw limit.

By itself, the GNM is an appealing model of neutrino masses which postulates the existence of only a single heavy neutrino to accommodate neutrino masses and mixings, while the other models require at least two additional fields. The GNM is then particularly attractive in the tiny seesaw parameter region: it has less particles and, because of the approximate (but not exact) Z_2 symmetry, it can express the main phenomenological features of both the scotogenic and the scoto-seesaw models of the cLFV processes and the neutrino sector. Investigating this parameter region we will address the following question in this paper: Which restrictions are imposed by the cLFV on the scalar sector in the GNM?

In section 2, we give an overview of the GNM by introducing the scalar and Yukawa sectors. Then we present the one-loop neutrino mass calculation. It leads to a parameterization of the flavor basis Yukawa couplings, similar to the Casas-Ibarra parameterization [44] that automatically reproduces neutrino masses and mixings at one-loop level. We close the section by noting the existing special parameter points in this parameterization, the checks, the numerical stability, and the limitations of our study, using FlexibleSUSY [45–47]. In section 3 we present the analytical expressions for cLFV processes. In section 4 we give a short recap of the most important parameters from the Yukawa sector and the scalar sector that control the branching ratios of cLFV processes and we lay out the strategy of our phenomenological study. We then pursue this strategy in section 5, give an interpretation of the results, and conclude our study in section 6. Technical details, such as the explicit derivation of the parametrization, peculiarities of the minimal free parameter set in the Yukawa sector, and the numerical values of some special cases can be found in the appendices.

2 The Grimus-Neufeld model

The GNM is a general 2HDM extended with one single sterile neutrino. In the limit of the *tiny seesaw scale* discussed below, the Yukawa sector is approximately Z_2 symmetric [42], thus its predictions for cLFV become similar to the scotogenic and scoto-seesaw models. Scotogenic and the scoto-seesaw models also predict scalar Dark matter (DM), which is a direct consequence of the Z_2 symmetry. The approximate Z_2 symmetry in the GNM will make the potential scalar DM candidate in the GNM not as stable. Yet to be sure if GNM has a viable DM candidate in this scenario, a dedicated analysis is needed, which is beyond the scope of this work. We do not discuss DM in this paper.

2.1 Scalar and Yukawa sectors

In principle, cLFV in the GNM can be analyzed for a general 2HDM scalar sector. However, to highlight the similarities between models we consider the scalar potential to be Z_2 symmetric. The Higgs sector of the model contains two Higgs doublets $H_{1,2}$. The potential takes the form:

$$V = m_{11}^2 H_1^\dagger H_1 + \frac{\lambda_1}{2} (H_1^\dagger H_1)^2 + m_{22}^2 H_2^\dagger H_2 + \frac{\lambda_2}{2} (H_2^\dagger H_2)^2 + \lambda_3 (H_1^\dagger H_1)(H_2^\dagger H_2) + \lambda_4 (H_2^\dagger H_1)(H_1^\dagger H_2) + \left[\frac{\lambda_5}{2} (H_2^\dagger H_1)^2 + h.c. \right]. \quad (2.1)$$

Only the first Higgs doublet H_1 acquires a vacuum expectation value (VEV) v , and we parametrize the two doublets as:

$$H_1 = \begin{pmatrix} G_W^+ \\ \frac{1}{\sqrt{2}}(v + h + iG_Z) \end{pmatrix}, \quad H_2 = \begin{pmatrix} H^+ \\ \frac{1}{\sqrt{2}}(H + iA) \end{pmatrix}. \quad (2.2)$$

All the SM particles, including H_1 , are assigned an even parity under the Z_2 symmetry, while H_2 and the additional sterile neutrino N are odd.¹ The latter enters the Lagrangian with, in general, complex Majorana mass term M and new Yukawa-like coupling $Y_j^{(i)}$ to the $SU(2)$ lepton doublets ℓ_j , where j denotes the generation:

$$\mathcal{L} \ni -\frac{1}{2}MNN - Y_j^{(i)}\ell_j\epsilon H_i N + h.c. \quad (2.3)$$

The matrix $\epsilon = i\sigma_2$ combines the two doublets to an $SU(2)$ invariant product. The Majorana mass M is made real by adjusting the phase of N . Terms with the neutrino Yukawa couplings $Y^{(1)}$ to the first Higgs doublet in eq. (2.3) explicitly break the Z_2 symmetry. The SM-like Z_2 -preserving Yukawa sector reads as:

$$\mathcal{L} \ni -Y_{kj}\tilde{H}_1\epsilon\ell_j e_k^c + h.c. \quad (2.4)$$

Note the usage of $\tilde{H}_1 = \epsilon H_1^*$ allowing for another $SU(2)$ invariant product with opposite electric charge. In the flavor basis charged lepton masses are defined by $Y_{ff} = \sqrt{2}m_f/v$, $f = e, \mu, \tau$, which is also the mass eigenstate basis for charged leptons, but not the mass eigenstate basis for neutrinos.

When the Higgs acquires a VEV, the Lagrangian in eq. (2.3) leads to the two non-vanishing Majorana masses for neutrinos, light m_3 and heavy m_4 (in mass eigenstate basis):

$$\mathcal{L} \ni -\frac{1}{2}m_3\nu'_3\nu'_3 - \frac{1}{2}m_4\nu'_4\nu'_4, \quad (2.5)$$

where

$$y^2 := \sum_i |Y_i^{(1)}|^2 = \frac{2m_3m_4}{v^2}, \quad M = m_4 - m_3, \quad (2.6)$$

which is the usual type-I seesaw mechanism relating the Yukawa coupling $Y_i^{(1)}$, the light neutrino mass m_3 , and the seesaw scale $m_4 \gg m_3$. The m_3 mass is associated with a light

¹For fermions we use the notation of two component Weyl spinors.

neutrino mass and is of $O(0.01 \text{ eV})$. If $y \rightarrow 0$ for fixed m_4 then $m_3 \rightarrow 0$, and the seesaw mechanism is “turned off” for the exact Z_2 symmetry. For $y \neq 0$, the seesaw mechanism applies, and for fixed m_3 , eq. (2.6) can be treated as a relationship between the seesaw scale and the Z_2 breaking parameter, allowing us to define an approximate Z_2 symmetry in the GNM by the inequalities:

$$m_4 \lesssim 10 \text{ GeV} \quad \Leftrightarrow \quad y \lesssim 10^{-7}. \quad (2.7)$$

The restriction of eq. (2.7) ensures that the Z_2 -breaking Yukawa coupling is at least an order of magnitude smaller than the Yukawa coupling of the electron.

There are at least two non-vanishing masses for light neutrinos. In the GNM the mass of the other SM neutrino is generated at one-loop level via interactions with H_2 . Motivated by a broken Peccei-Quinn symmetry, small λ_5 values successfully generate radiative neutrino masses with relatively large Yukawa couplings to the second Higgs doublet, namely $Y^{(2)}$. Just as the limit $y \rightarrow 0$ turns off the seesaw mechanism, setting $\lambda_5 \rightarrow 0$ turns off the radiative mass generation leaving one of the needed neutrino masses unexplained. In the GNM the lightest neutrino is massless.

The Z_2 symmetry in the Yukawa sector leads to the similarity between the GNM, the scotogenic, and the scoto-seesaw models in the cLFV phenomenology, even though the Yukawa sectors are slightly different. The scotogenic model [21] has an exact Z_2 symmetry, forcing $y \rightarrow 0$ and turning off the seesaw mechanism at the cost of adding 2 additional heavy, Z_2 -odd neutrino states. Then the Yukawa couplings $Y^{(2)}$, which lead to radiative mass generation, are contained in a 3×3 matrix instead of a 3×1 as in the GNM.

In the scoto-seesaw model [32, 33], one has an exact Z_2 symmetry turning off the seesaw mechanism for the Z_2 -odd N , at the cost of adding one Z_2 -even sterile neutrino, for which, only the seesaw mechanism is allowed. This effectively gives one additional independent parameter, the mass of the Z_2 -even neutrino in contrast to the GNM. In turn, this allows to control the sizes of parameters that enter the radiative and the seesaw mass mechanisms independently from each other in the scoto-seesaw model, while they are related in GNM.

In the GNM, the two SM-like massive neutrino mass states mix in general. To get a convenient parameterization for the Yukawa couplings, one solves the equations for neutrino masses and mixings at one-loop level. We further describe the needed rotations, convenient basis and neutrino mass generation in GNM leading to this parameterization in detail in the following sub-sections.

2.2 Rotations for neutrinos

The GNM contains four neutrino states, comprised of the three neutrino components ν_i of the lepton doublets, and the single sterile neutrino N . At tree level, neutrino masses arise from the Majorana mass term M and the Yukawa coupling vector $Y^{(1)}$, coupling the neutrino states to the VEV. These tree-level mass terms of eq. (2.3) give rise to the 4×4 neutrino mass matrix M_ν^F in flavor basis $\{\nu_i, N\}$ as shown with the first matrix in

$$\begin{array}{ccc}
\begin{pmatrix} 0_{3 \times 3}^{0\ell} & \frac{v}{\sqrt{2}} Y^{(1)} \\ \frac{v}{\sqrt{2}} Y^{(1)T} & M \end{pmatrix} & \xrightarrow{\tilde{V}} & \begin{pmatrix} 0^{1\ell} & 0^{1\ell} & 0^{1\ell} & 0^{1\ell} \\ 0^{1\ell} & 0^{0\ell} & 0^{0\ell} & 0^{0\ell} \\ 0^{1\ell} & 0^{0\ell} & 0^{0\ell} & i \frac{vy}{\sqrt{2}} \\ 0^{1\ell} & 0^{0\ell} & i \frac{vy}{\sqrt{2}} & M \end{pmatrix} & \xrightarrow{\tilde{S}} & \begin{pmatrix} 0^{1\ell} & 0^{1\ell} & 0^{1\ell} & 0^{1\ell} \\ 0^{1\ell} & \hat{\Sigma} & 0^{1\ell} & \\ 0^{1\ell} & & 0^{1\ell} & \\ 0^{1\ell} & 0^{1\ell} & 0^{1\ell} & m_4 + 0^{1\ell} \end{pmatrix} & \xrightarrow{\tilde{R}} & \hat{m} \\
\parallel & & & & & \parallel \\
M_\nu^F & & & & & \tilde{U}^* M_\nu^F \tilde{U}^\dagger \\
\nu_\alpha := \{\nu_i, N\} & & \nu'_\alpha & \approx & \nu'_\alpha & \nu''_\alpha \\
Y^{(i)} & & Y^{(i')} & \approx & Y^{(i')} & Y^{(i'')}
\end{array}$$

Figure 1: A sequence of rotations for neutrino mass matrix M_ν^F . Explicit entries show quantities used in the paper. We denote an expression that is zero exactly at tree-level by $0^{0\ell}$. With $0^{1\ell}$ we mean an approximated one-loop zero, where terms proportional to $y^2 \times \text{loop}$ and $\frac{m_3}{m_4} \times \text{loop}$ are neglected. The matrix $\hat{\Sigma}$ contains non-vanishing expressions for the processes $\nu'_i \rightarrow \nu'_j$ at one-loop level, which are not further suppressed by y^2 or $\frac{m_3}{m_4}$.

figure 1. To find the physical neutrino states and their masses, one has to include one-loop corrections and diagonalize the mass matrix by unitary transformations.²

The mass matrix M_ν^F is diagonalized by a unitary matrix \tilde{U} to a diagonal matrix \hat{m} , see figure 1. The diagonalization matrix \tilde{U} can be decomposed into a product of three unitary matrices:

$$\tilde{U}^* M_\nu^F \tilde{U}^\dagger := \tilde{R}^* \tilde{S}^* \tilde{V}^* M_\nu^F \tilde{V}^\dagger \tilde{S}^\dagger \tilde{R}^\dagger =: \hat{m}. \quad (2.8)$$

This decomposition is useful because each rotation leads to a separate physical consequence or highlights important details about the Yukawa couplings. The sequence of these three rotations and their effect on the mass matrix is schematically shown in figure 1. In the following, we will discuss the diagonalization steps in more detail. It will be useful to introduce the decomposition of the relevant 4×4 matrices as:

$$\tilde{U} \approx \begin{pmatrix} U & 0 \\ 0 & 1 \end{pmatrix}, \quad \tilde{V} = \begin{pmatrix} V & 0 \\ 0 & 1 \end{pmatrix}, \quad \tilde{R} = \begin{pmatrix} R & 0 \\ 0 & 1 \end{pmatrix}, \quad R = \begin{pmatrix} 1 & 0 \\ 0 & \hat{R} \end{pmatrix}, \quad (2.9)$$

where U , V and R are 3×3 unitary matrices and \hat{R} is a 2×2 unitary matrix. We will define the matrix \tilde{S} in eq. (2.12) and explain the approximate equality right after eq. (2.14).

In the Lagrangian of eq. (2.3) new complex Yukawas $Y^{(i)}$ are introduced, which carry 12 degrees of freedom in total. As the first step of the diagonalization process we use the freedom to rotate flavor neutrinos ν_α to choose a convenient basis. This is done by the

²Our conventions for unitary rotations are the ones of ref. [48], as implemented in FlexibleSUSY:

$$\text{for } UU^\dagger = \mathbb{1}: \quad \psi_k^{old} = U_{ik}^* \psi_i^{new}, \quad m \stackrel{\text{Takagi}}{=} U^T m_{diag} U, \quad m \stackrel{\text{SVD}}{=} U_1^T m_{diag} U_2.$$

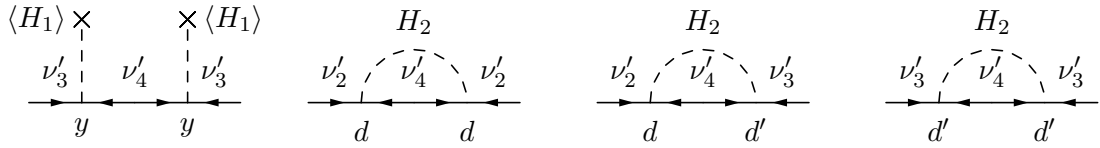


Figure 2: Diagrams, contributing to the $\hat{\Sigma}$ mass matrix. Arrows show the flow of chirality.

matrix V in the following way:

$$\left. \begin{aligned} Y_j^{(1)} V_{ij}^* &= \{0, 0, iy\}_i =: Y_i^{(1)} \Leftrightarrow 5 \text{ conditions,} \\ Y_j^{(2)} V_{ij}^* &= \{0, d, id'\}_i =: Y_i^{(2)} \Leftrightarrow 3 \text{ conditions.} \end{aligned} \right\} \text{ with } y, d > 0, d' \in \mathbb{C}, \quad (2.10)$$

i.e. the two Yukawa vectors $Y^{(i)}$ are transformed into two positive and one complex parameter y, d, d' . Thus the 8 degrees of freedom of the unitary matrix V are determined by lhs. of eq. (2.10), while the remaining 4 are shown in the rhs. of eq. (2.10). The only unfixed degree of freedom in a matrix V is a single phase:

$$V \rightarrow \text{diag}(e^{i\alpha_1}, 1, 1)V. \quad (2.11)$$

This phase, α_1 , is used to absorb one of the Majorana phases η_i of the Pontecorvo-Maki-Nakagawa-Sakata (PMNS) matrix. Additionally, 3 degrees of freedom in V can be absorbed into the phase definitions of neutrinos, leading to 5 physical degrees of freedom in V , which are later related to the 3 angles, 1 CP phase, and 1 Majorana phase of the PMNS matrix. 2 of the 4 degrees of freedom of the rhs. of eq. (2.10) will be related to neutrino masses.

It is clear from eq. (2.10) that one of the neutrinos doesn't interact with the Higgs bosons after the rotation \tilde{V} , which leads to vanishing contributions to its mass at tree level and at one-loop level. These vanishing elements of the mass matrix are shown by $0^{1\ell}$ in the top and left outer entries of the matrices in figure 1.

At the second step of figure 1, the tree-level mass matrix has a typical seesaw structure. Correspondingly, the second diagonalization matrix \tilde{S} is a tree-level seesaw transformation, which yields a diagonal mass matrix at tree level with two non-vanishing tree-level mass eigenvalues m_3 and m_4 , related by eq. (2.6). The appropriate seesaw rotation \tilde{S} can be written as:

$$\tilde{S} := \begin{pmatrix} \mathbb{1} & 0 \\ 0 & c_S \quad is_S \\ & is_S \quad c_S \end{pmatrix}, \quad \text{with } c_S = \sqrt{\frac{m_4}{m_4 + m_3}}, \quad s_S = \sqrt{\frac{m_3}{m_4 + m_3}}. \quad (2.12)$$

After this diagonalization step, we take into account one-loop corrections to the masses. Since one of the neutrinos does not couple to the Higgs bosons, the one-loop neutrino mass corrections lead to the block structure indicated in the third matrix of figure 1: the two non-vanishing blocks at the level of our approximation are the 2×2 mass matrix block $\hat{\Sigma}$, which contains the tree-level eigenvalue m_3 and one-loop self-energy corrections, and the heavy seesaw neutrino mass m_4 . All other entries are either generated at higher loops

or are neglected in one-loop diagrams as being either proportional to $y^2 \times \text{loop}$, which is extremely small in our case (see eq. (2.7)), or to $\frac{m_3}{m_4} \times \text{loop}$, which has an additional seesaw suppression factor. As will be shown in the next section, the last rotation \hat{R} diagonalizes $\hat{\Sigma}$ and can be used to parameterize the Yukawas couplings $Y^{(i\prime)}$ in the mass eigenstate basis. Its form will be described in eq. (2.21).

There are in total three non-zero masses for neutrinos at one-loop level. We write them in the ascending order as:

$$\hat{m} := \text{diag}(0, m_2^{\text{pole}}, m_3^{\text{pole}}, m_4), \quad (2.13)$$

where we consider the loop corrections for the heaviest mass to be negligible. Also, $m_4 \gg m_3$ leads to

$$\tilde{U} = \tilde{R}\tilde{S}\tilde{V} \approx \tilde{R}\tilde{V} \Rightarrow U \approx RV, \quad (2.14)$$

which means that neutrino masses and mixings can be related to the so-called 3ν mixing paradigm $|\tilde{U}_{i4}| \ll 1$, which was indicated in the definition of \tilde{U} in eq. (2.9). The PMNS matrix is defined as [49]:

$$U_{\text{PMNS}} = \begin{pmatrix} 1 & 0 & 0 \\ 0 & c_{23} & s_{23} \\ 0 & -s_{23} & c_{23} \end{pmatrix} \begin{pmatrix} c_{13} & 0 & s_{13}e^{-i\delta_{\text{CP}}} \\ 0 & 1 & 0 \\ -s_{13}e^{i\delta_{\text{CP}}} & 0 & c_{13} \end{pmatrix} \begin{pmatrix} c_{12} & s_{12} & 0 \\ -s_{12} & c_{12} & 0 \\ 0 & 0 & 1 \end{pmatrix} \begin{pmatrix} e^{i\eta_1} & 0 & 0 \\ 0 & e^{i\eta_2} & 0 \\ 0 & 0 & 1 \end{pmatrix}, \quad (2.15)$$

where η_1 and η_2 are unknown Majorana phases, $s_{ij} = \sin \theta_{ij}$, and $c_{ij} = \cos \theta_{ij}$, see eq. (2.18). In the GNM, the lightest neutrino has a vanishing mass and the phase η_1 can be absorbed into a redefinition of the corresponding field, as shown in eq. (2.11). Hence only η_2 is physical. To keep our study simple, and since there is no evidence of η_2 in the PMNS matrix so far, we set it to zero. The zero-mass lightest neutrino also implies a lower bound on neutrinoless double-beta decay [50], which is however left out of the scope of this paper.

The pole masses in eq. (2.13) are different for Normal ordering (NO) and Inverted ordering (IO). Since the mass of the lightest neutrino vanishes, the measured mass squared differences from the neutrino oscillation experiments determine the actual neutrino masses. Therefore, eq. (2.8) connects the PMNS matrix with U , which we can summarize as:

$$\begin{aligned} \text{NO: } m_2^{\text{pole}} &= \sqrt{\Delta m_{21}^2}, & m_3^{\text{pole}} &= \sqrt{|\Delta m_{32}^2| + \Delta m_{21}^2}, & U &= U_{\text{PMNS}}^\dagger, \\ \text{IO: } m_2^{\text{pole}} &= \sqrt{|\Delta m_{32}^2| - \Delta m_{21}^2}, & m_3^{\text{pole}} &= \sqrt{|\Delta m_{32}^2|}, & U &= O_{\text{IO}} U_{\text{PMNS}}^\dagger, \end{aligned} \quad (2.16)$$

where the sign convention for Δm_{32}^2 is explicitly avoided, and the mass ordering of IO is related to the usual 3ν conventions by:

$$O_{\text{IO}} = \begin{pmatrix} 0 & 1 \\ \mathbb{1}_{2 \times 2} & 0 \end{pmatrix}. \quad (2.17)$$

We take as numerical values in our code from ref. [49]:

$$\begin{aligned} \Delta m_{21}^2 &= 7.4 \cdot 10^{-5} \text{ eV}^2, & |\Delta m_{32}^2| &= 2.5 \cdot 10^{-3} \text{ eV}^2, \\ \theta_{12} &= 0.59 \text{ rad}, & \theta_{23} &= 0.84 \text{ rad}, & \theta_{13} &= 0.15 \text{ rad}, & \delta_{\text{CP}} &= 4.5 \text{ rad}, \end{aligned} \quad (2.18)$$

where δ_{CP} is taken from the intersection of measured 1σ -regions for NO and IO scenarios.

2.3 Neutrino mass matrix

The Yukawa interactions introduced in eq. (2.3) can be parameterized by four real parameters, as shown in eq. (2.10). One can connect them with the definition of the unitary 2×2 rotation \hat{R} and use the compact parameters of the latter instead. This section provides the required relations.

The light neutrino mass matrix $\hat{\Sigma}$ disentangles from the heavy one due to eq. (2.14), see ref. [51] and figure 1. The interactions with the doublet H_1 are proportional to the Yukawa coupling $y \sim |Y^{(1)}|$ in eq. (2.7), which we assume to be vanishingly small due to the approximate Z_2 symmetry. The relevant contributions to $\hat{\Sigma}$ are shown in figure 2:

$$\hat{\Sigma} \approx \begin{pmatrix} 0 & 0 \\ 0 & m_3 \end{pmatrix} + \Lambda \begin{pmatrix} d^2 & idd' \\ idd' & -d'^2 \end{pmatrix}, \quad \Lambda := \frac{m_4}{32\pi^2} [B_0(0, m_4^2, m_A^2) - B_0(0, m_4^2, m_H^2)] \quad (2.19)$$

with the loop contribution similar to the scotogenic model [21], and the definition of Λ as in ref. [52].³ The diagonalization of $\hat{\Sigma}$ is done via the Takagi decomposition:

$$\hat{R}^* \hat{\Sigma} \hat{R}^\dagger = \text{diag}(m_2^{\text{pole}}, m_3^{\text{pole}}), \quad (2.20)$$

which restricts the matrix \hat{R} , as shown in appendix A, due to the zero determinant of the one-loop correction term. For the rotation itself Murnaghan's parameterization is used:

$$\hat{R} = \begin{pmatrix} R_{22} & -R_{32}^* e^{i\phi_R} \\ R_{32} & R_{22}^* e^{i\phi_R} \end{pmatrix}, \quad \text{with} \quad R_{22} := \cos r e^{i\omega_{22}}, \quad R_{32} := \sin r e^{i\omega_{32}}. \quad (2.21)$$

The following ranges of angles and phases define the *rotation* in a unique way:

$$\phi_R, r \in [-\pi, \pi), \quad \omega_{22}, \omega_{32} \in \left[-\frac{\pi}{2}, \frac{\pi}{2}\right]. \quad (2.22)$$

The parameter ranges that uniquely describe cLFV ratios are smaller:

$$r, \omega_{22} \in \left(-\frac{\pi}{2}, \frac{\pi}{2}\right], \quad (2.23)$$

which is derived in appendix B.

The four degrees of freedom — m_3 , d and complex d' — are replaced by the two neutrino pole masses $m_{2,3}^{\text{pole}}$ and the rotation matrix parameters r and ω_{22} . The other parameters of \hat{R} are fixed by eq. (2.20). In this paper we take the point of view that very large one-loop corrections for m_3 are fine tuned and unnatural: hence we only analyze parameter regions where they do not exceed 50%, which corresponds to the following range for m_3 :

$$m_2^{\text{pole}} < m_3 < 2m_3^{\text{pole}}. \quad (2.24)$$

It is convenient to define the abbreviation t_{32} , representing the ratio between the two physical neutrino masses:

$$t_{32} := \frac{m_3^{\text{pole}}}{m_2^{\text{pole}}} \approx \begin{cases} 5.898 & \text{for NO} \\ 1.015 & \text{for IO} \end{cases}. \quad (2.25)$$

³The expression for Λ given in ref. [30] is two times larger, which looks like a direct equivalence to eq. (11) of ref. [21]. However, the definitions of the Yukawa couplings in these references differ by $\sqrt{2}$, which should lead to additional factor of one half for Λ in ref. [30]. Hence, there might be a typo in the neutrino Yukawa couplings in ref. [30]: they are by a factor of $\sqrt{2}$ smaller then required.

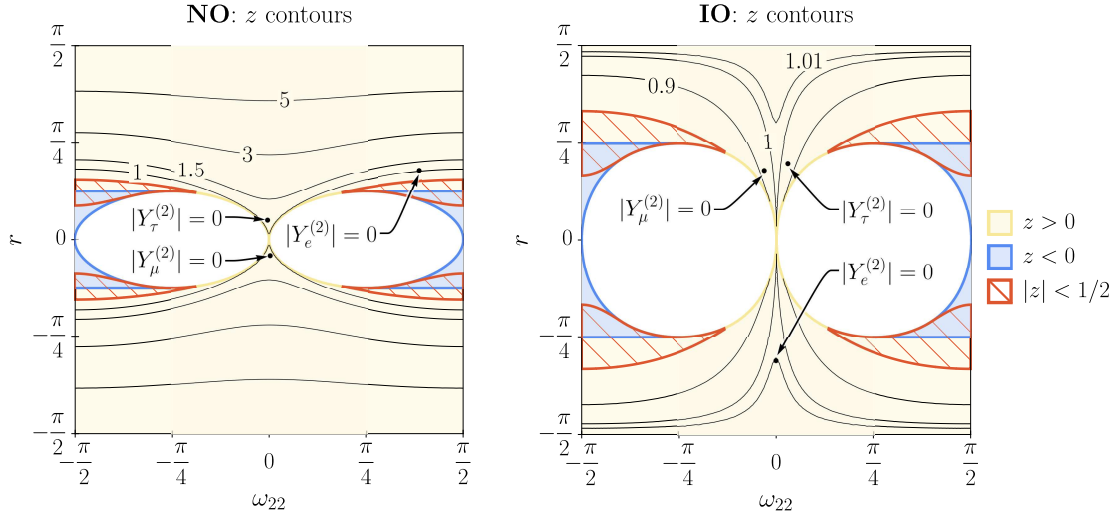


Figure 3: Parameter regions of the $\omega_{22} - r$ plane, representing two out of the four physical input parameters of the model r , ω_{22} , m_4 and $|\Lambda|$. The definition of z , eq. (2.26), is essential for the restrictions of ω_{22} and r , as it has to be real, as discussed in appendix B. The white areas are excluded by not fulfilling eq. (B.7). The contours of the values of z are in the range allowed by eq. (2.27), except for the red striped region, where $|z| < \frac{1}{2}$, which we exclude as being fine-tuned. These red striped areas will also be colored white in later plots, as we will not consider this parameter region for the discussed exclusion criteria. The points where the second Yukawa coupling to electrons, muons, or taus vanish exactly are also shown for both hierarchies.

It is also convenient to define the parameter z by

$$z(r, \omega_{22}, \omega_{32}) = \cos^2 r e^{2i\omega_{22}} + t_{32} \sin^2 r e^{2i\omega_{32}}. \quad (2.26)$$

Using (A.5) we see that z corresponds to the relative loop contribution to the neutrino mass m_3 , and we can express eq. (2.24) in terms of these parameters:

$$z \in \mathbb{R}, \quad |z| = \frac{m_3^{\text{pole}}}{m_3} \Rightarrow 0.5 < |z| < t_{32}. \quad (2.27)$$

From eqs. (2.26, 2.27) we determine ω_{32} . There are three regions of possible solutions of eq. (2.27) for ω_{32} to be used in the parameterization. However, these solutions lead to physically equivalent Yukawa couplings, as shown in appendix B, thus we use

$$\omega_{32} := -\frac{1}{2} \arcsin \left(\frac{\sin(2\omega_{22})}{t_{32} \tan^2 r} \right). \quad (2.28)$$

The region for the parameters r and ω_{22} satisfying the constraint of eq. (2.27) is shown in figure 3 as colored regions, while white regions are disallowed.

With these definitions, we can determine the Yukawa couplings $Y^{(i)}$ in the one-loop mass eigenstate basis, which reproduce the PMNS matrix and the neutrino masses by

construction. The following Yukawa couplings follow from eq. (2.20):

$$Y^{(2'')} := \text{sign}(\Lambda) \sqrt{\frac{m_2^{\text{pole}}}{|z\Lambda|}} (0, R_{22}, t_{32}R_{32}), \quad (2.29)$$

$$Y^{(1'')} := \frac{i}{e^{i\phi_R}} \sqrt{\frac{2m_3^{\text{pole}}m_4}{|z|v^2}} (0, -R_{32}, R_{22}). \quad (2.30)$$

Inserting eq. (2.28) into eqs. (2.21, 2.26, 2.29, 2.30) leads to a parameterization of the Yukawa couplings as functions $Y^{(1'')}(r, \omega_{22}, m_4)$ and $Y^{(2'')}(r, \omega_{22}, \Lambda)$. For cLFV, the Yukawa coupling to the first Higgs doublet, eq. (2.30), can be neglected in the tiny seesaw scenario, thus only $Y^{(2'')}(r, \omega_{22}, \Lambda)$ will contribute to cLFV.

Changing the sign of Λ changes the phase of $Y^{(2'')}$. But this phase cancels in the calculation of cLFV decays. This means that cLFV observables restrict only the absolute value of Λ . The relation between mass eigenstate Yukawa couplings $Y^{(i'')}$ of eqs. (2.30, 2.29) and the flavor ones $Y^{(i)}$ is given by:

$$Y^{(i)} = Y^{(i'')}U. \quad (2.31)$$

The rotation U is related to the PMNS matrix in eq. (2.16). With the Yukawa coupling of eq. (2.29) this resembles the Casas-Ibarra parameterization, ref. [44], adapted for the scotogenic model, ref. [30]. Setting $m_3^{\text{pole}} \rightarrow 0$ in eq. (2.29) realizes the exact equality.

2.4 Vanishing $Y^{(2)}$

Neutrinos contribute to cLFV processes via Yukawa couplings to the second Higgs doublet, $Y^{(2)}$. Hence, the vanishing Yukawa coupling leads to a vanishing neutrino contribution to the process of interest. It turns out, there are solutions that simultaneously give a vanishing Yukawa coupling in the flavor basis and reproduce neutrino masses and mixings. Using eqs. (2.21, 2.29, 2.31) and setting $Y_f^{(2)} = 0$ for a given flavor f one gets:

$$\cot(r)e^{i(\omega_{22}-\omega_{32})} = -t_{32}\frac{U_{3f}}{U_{2f}}, \quad (2.32)$$

where the solution for ω_{32} of eq. (2.28) is used. The complex equation (2.32) gives a single solution in NO or IO for each flavor f (and it depends only on ω_{22} and r). These points of vanishing $Y^{(2)}$ in the $\omega_{22} - r$ plane are shown in figure 3 as dots with corresponding callouts, and their numerical values are given in appendix D.

The solutions of eq. (2.32) are not backed by any fundamental reasoning, are not stable and are fine-tuned. Nevertheless, these solutions do exist and, if the small parameter ranges around them are included, they will lead to weaker constraints on the scalar sector for cLFV. Thus, if we discard some tiny parameter region around these points, we would make our main result, a constraint on the scalar sector from cLFV, dependent on our own choice of the size of the region. Instead, we choose a more agnostic approach: we include it, discuss it in more detail, and provide a suggestion of how one can define a “more likely” scenario away from these regions and a “fine-tuned” one around these regions. In this way, we completely cover the full parameter space of the model and do not make our main result dependent on additional assumptions.

2.5 Reproducing neutrino masses and mixings

To realize the numerical scans over model parameters we used the `FlexibleSUSY` [45–47] spectrum-generator generator, including the extension `NPointFunctions` [53]. It allowed us to straightforwardly implement the non-trivial mass-generation mechanism for neutrino masses in the GNM, combining tree- and loop-level generated masses, as well as the experimentally measured PMNS mixing matrix. In particular, we created `SARAH` [54, 55] model files for the realization of the GNM studied in this paper. In addition, we designed the `FlexibleSUSY` model file incorporating the parameterization of the parameter space developed in section 2.⁴ This working setup also resulted in an independent cross-check of the consistency of our analytical one-loop parameterization of the neutrino sector.

However, using the current implementation of the code `FlexibleSUSY` we spotted a bug in the neutrino pole mass calculation, where the couplings in self-energies taken from `SARAH` were conjugated, compared to analytical expressions both done by hand and with `FeynArts` [56] and `FormCalc` [57]. As a workaround, the conjugation of self-energies in the neutrino pole mass calculation in `FlexibleSUSY` was applied.

For the studied tiny seesaw parameter region, the elements of the PMNS matrix and the output neutrino masses at one-loop are consistent within 1% accuracy. However, for some limiting cases that lie beyond the region of our interest, the description ceases to be accurate enough.

Since we study a tiny seesaw region, scale differences in the neutrino sector are limited only to 12 orders of magnitude ($m_4 \approx 10$ GeV vs. $m_2 \approx 10^{-11}$ GeV). This helps us in numerical stability. In fact, we checked that for a seesaw scale of $m_4 > 10$ GeV, the neutrino mixing matrix in `FlexibleSUSY` becomes inaccurate ($>1\%$), while for the neutrino masses the scale is higher $m_4 > 100$ GeV. We find numerically stable and correct neutrino masses and mixings, allowing up to 1% deviation in the output of `FlexibleSUSY`, for

$$\Lambda > m_3^{\text{pole}} \approx 5 \cdot 10^{-11} \text{ GeV}. \quad (2.33)$$

It is interesting to note that this limiting value gives the largest Yukawa coupling with value $Y^{(2)} \approx O(1)$. Hence, the Yukawa values higher than $O(1)$ and up to a perturbativity limit do not accurately reproduce the neutrino spectrum in `FlexibleSUSY` for this model. For our study, however, we will not reach this scenario since cLFV gives stronger constraints in general. This means that all our results are consistent, cross-checked, and reproducible with `FlexibleSUSY`.⁵

3 Charged Lepton Flavor Violating processes

The new Yukawa interactions are not only responsible for the generation of neutrino masses, but they also give rise to cLFV. In this section we provide the theoretical formulas for the amplitudes of two-body decays $l_i \rightarrow l_j \gamma$, $\mu \rightarrow e$ conversion (valid for all nuclei), and three-body decays $l_i \rightarrow l_j l_k l_k^c$. First, we present Feynman diagrams and the amplitudes,

⁴The mentioned files are available on the preprint web page for this paper.

⁵After correcting the mentioned issue of Majorana pole mass calculation in `FlexibleSUSY`.

specifying relevant and negligible ones. Later, the amplitudes are combined into the decay (and conversion) rates. The numerical calculations are also implemented in `FlexibleSUSY`, using the additional extension `NPointFunctions` [53].

3.1 Coefficients

Let us start from the simplest case of the penguin contributions, see the Feynman diagrams in figure 4. We express the amplitude of the flavor-changing decay $l_i \rightarrow l_j \gamma$ into an off-shell photon with *outgoing* momenta $q = p_i - p_j$ as in ref. [58]:

$$i\Gamma_{\bar{l}_j l_i \gamma} = i\bar{u}_j \left[(q^2 \gamma^\mu - q^\mu \not{q}) (A_1^L P_L + A_1^R P_R) + im_i \sigma^{\mu\nu} q_\nu (A_2^L P_L + A_2^R P_R) \right] u_i. \quad (3.1)$$

For the considered scenario in the GNM, the dominant photon contribution is given by one-loop diagrams of figures 4b-4d with virtual charged Higgs boson H^- and virtual Majorana neutrino ν_4'' exchange. In these diagrams, the lepton flavor transition is mediated by the new Yukawa coupling $Y^{(2)}$.

Other contributions are negligible due to the following reasons. The impact of Goldstone bosons $G_{\tilde{W}}^-$ is suppressed by the Z_2 -breaking Yukawa coupling $|Y^{(1)}| \ll 1$. The impact of vector bosons is suppressed due to the Glashow-Iliopoulos-Maiani (GIM) mechanism which leads to a $m_{\nu_i}^2/m_W^2$ factor and to terms proportional to $|\tilde{U}_{i4}| \ll 1$. Also, in our scenario, for other cLFV processes under consideration, one can always neglect the electron Yukawa coupling $Y^{(1)}$ due to its small magnitude relative to $Y^{(2)}$.

The only non-vanishing coefficients in the decay rate, eq. (3.1), are the following:

$$A_1^L = \frac{Y_i^{(2)*} Y_j^{(2)}}{16\pi^2 m_{H^\pm}^2} \frac{e}{18} F_A\left(\frac{m_4^2}{m_{H^\pm}^2}\right), \quad A_2^R = \frac{Y_i^{(2)*} Y_j^{(2)}}{16\pi^2 m_{H^\pm}^2} \frac{e}{12} F_B\left(\frac{m_4^2}{m_{H^\pm}^2}\right) \quad (3.2)$$

with the loop functions given in eq. (3.5).

Another class of cLFV diagrams are Z -boson penguins, shown in figure 4. It turns out, that they can be removed from the consideration. The diagram in figure 4a is proportional to the $\nu_\alpha'' \nu_\beta'' Z$ coupling. Though this coupling does not vanish for the first three generations of neutrinos, flavor-changing couplings to external leptons include $\tilde{U}_{\alpha 4}$, which leads to a seesaw suppression. The diagrams of figures 4b-4c have non-vanishing couplings but they lead to the zero factor of $(B_1 + 2C_{00})$ with

$$B_1 = B_1(0, m_4^2, m_{H^\pm}^2), \quad C_{00} = C_{00}(0, 0, 0, m_4^2, m_{H^\pm}^2, m_{H^\pm}^2). \quad (3.3)$$

The last diagram in figure 4d is proportional to $Y^{(1)}$. Overall, this discussion shows that the impact of Z -penguins is negligible for our scenario. Similarly, the Higgs boson penguin is suppressed by Yukawa couplings to charged leptons. From this follows, that only the photon penguin gives a non-vanishing contribution.

Next, we consider box contributions relevant for $l_i \rightarrow l_j l_k^c l_k^c$, see figures 5a-5d. They sum up to the result:

$$A_{\text{box}}^{LL} = \frac{Y_i^{(2)*} Y_j^{(2)}}{16\pi^2 m_{H^\pm}^2} \frac{|Y_k^{(2)}|^2}{2} F_C\left(\frac{m_4^2}{m_{H^\pm}^2}\right), \quad \text{with } Y_{ee} \approx 0, \quad \text{and } Y_{kk} \ll Y_k^{(2)}. \quad (3.4)$$

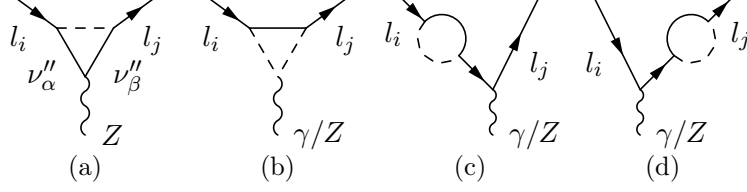


Figure 4: Feynman diagrams for γ and Z contributions to cLFV processes for two- and three-body decays. Contributions for two-body decays have an on-shell γ on the external line, while contributions for three-body decays have off-shell γ and Z on the external line, which should be understood as subdiagrams of full penguin diagrams. Arrows represent the propagation of particles; scalars and fermions lines in the loops correspond to H^- and ν_4'' . The only non-negligible contribution comes from the photon diagram in figure 4b. Figures 4c-4d do not give numerically meaningful contribution, but they have to be included to ensure that UV divergences cancel exactly. All the diagrams that include Z boson are negligible, while the diagram shown in figure 4a is zero for a photon contribution.

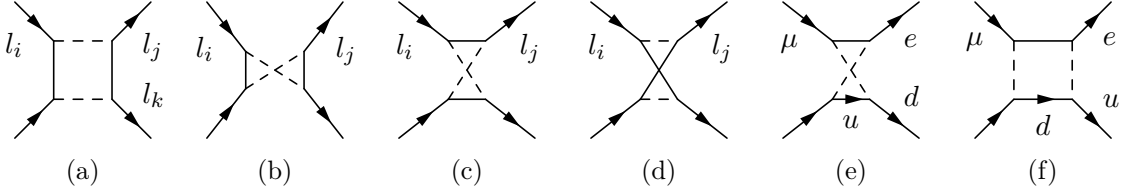


Figure 5: Box contribution. The first two four-lepton diagrams from the left are proportional to $m_4^2 D_0$, the last two of them — to $2D_{00}$. Arrows represent the propagation of particles; scalar and fermion lines in the loops correspond to H^- and ν_4'' .

For the $\mu \rightarrow e$ conversion in presence of a nucleus, there are relevant box diagrams as well, see figures 5e-5f. They lead to a vanishingly small contribution, because in the GNM quarks are coupled to H_1 , leading to a $Y^{(1)}$ suppression in addition to the small Yukawa couplings.

The loop functions used above have the following form (see [59]):

$$\begin{aligned}
 F_A(x) &= \frac{1}{2(1-x)^4} (2 - 9x + 18x^2 - 11x^3 + 6x^3 \ln x), \\
 F_B(x) &= \frac{1}{(1-x)^4} (1 - 6x + 3x^2 + 2x^3 - 6x^2 \ln x), \\
 F_C(x) &= \frac{1}{(1-x)^3} (1 + 4x - 5x^2 + 2x(2+x) \ln x).
 \end{aligned}
 \tag{3.5}$$

The relevant limit for us is $|x| \ll 1$, and the loop functions are normalized as $F_i(x \rightarrow 0) = 1$.

Using eqs. (2.29, 2.31) one obtains for $m_4 \ll v \lesssim m_{H^\pm}$ that

$$A_1^L \propto \frac{1}{|\Lambda| m_{H^\pm}^2}, \quad A_2^R \propto \frac{1}{|\Lambda| m_{H^\pm}^2}, \quad A_{\text{box}}^{LL} \propto \frac{1}{\Lambda^2 m_{H^\pm}^2},
 \tag{3.6}$$

while the only other parameters that the amplitudes depend on are r and ω_{22} . This dependence is only slightly more complicated and can be read out from the Yukawa couplings.

Note, that the single parameter relating the scalar sector to the cLFV two-body decays is $|\Lambda|m_{H^\pm}^2$. This is also the most important factor for three-body decays because contributions from box diagrams can be neglected for $m_{H^\pm} \lesssim \text{TeV}$. In addition, the model predicts a very simple relationship between the two photonic amplitudes:

$$A_1^L \approx \frac{2}{3}A_2^R. \quad (3.7)$$

3.2 Decay widths

We use the following convention for a covariant derivative:

$$\mathcal{D}_\mu = \partial_\mu + ieQ_f A_\mu, \quad (3.8)$$

where $e > 0$ is the charge unit, Q_f the electric charge of a corresponding fermion f and A_μ the photon field.

The total decay width of $l_i \rightarrow l_j \gamma$ simplifies from eq. (3.1) to (see, e.g. [58, 59]):

$$\Gamma_{l_i \rightarrow l_j \gamma} = \frac{m_i^5}{16\pi} |A_2^R|^2. \quad (3.9)$$

The partial decay width with three leptons of the same generation in the final state is (see [60–62])

$$\begin{aligned} \Gamma_{l_i \rightarrow 3l_j} = \frac{m_i^5}{192\pi^3} & \left[e^2 |A_2^R|^2 \left(\ln \frac{m_i^2}{m_j^2} - \frac{11}{4} \right) + \frac{e}{2} \text{Re} [(2A_3^{LL} + A_3^{LR})A_2^{R*}] \right. \\ & \left. + \frac{1}{4} |A_3^{LL}|^2 + \frac{1}{8} |A_3^{LR}|^2 \right], \end{aligned} \quad (3.10)$$

where the u -channel for photon penguins is included via Fierz identities; for boxes, all channels are calculated directly, and the following abbreviations are used:

$$A_3^{LR} = -eA_1^L, \quad A_3^{LL} = -eA_1^L + \frac{1}{2}A_{\text{box}}^{LL}. \quad (3.11)$$

The minus sign for the photon penguin comes from the embedding into a four-fermion amplitude, and the factor 1/2 for the boxes comes from Fierz identities during the matching.

For three leptons of different generations in the final state, the expression for the partial decay rate differs [63]:

$$\begin{aligned} \Gamma_{l_i \rightarrow l_j l_k l_k^c} = \frac{m_i^5}{192\pi^3} & \left[e^2 |A_2^R|^2 \left(\ln \frac{m_i^2}{m_k^2} - 3 \right) + \frac{e}{2} \text{Re} [(A_4^{LL} + A_3^{LR})A_2^{R*}] \right. \\ & \left. + \frac{1}{8} |A_4^{LL}|^2 + \frac{1}{8} |A_3^{LR}|^2 \right] \end{aligned} \quad (3.12)$$

with different matching for boxes leading to an absence of the additional prefactor:

$$A_4^{LL} = -eA_1^L + A_{\text{box}}^{LL}. \quad (3.13)$$

For the conversion rate, we use [64]

$$\omega_{\mu \rightarrow e} = 4m_\mu^5 \left| \frac{1}{8} A_2^R D - eA_1^L V^{(p)} \right|^2 \quad (3.14)$$

with dimensionless integrals D and $V^{(p)}$ defined there as well. The minus sign reflects the different definition of the photon field that comes from the comparison of covariant derivatives.

4 Recap of important parameters

For our study we restrict the parameters:

$$m_4 \lesssim 10 \text{ GeV}, \quad m_{H^\pm} \lesssim 1 \text{ TeV}. \quad (4.1)$$

The first inequality rewrites the condition on the seesaw scale of eq. (2.7), the second one leads to charged Higgs boson masses well in reach of the LHC, and also leads to negligible box contributions in almost all of the parameter space and significantly simplifies the discussion.⁶

The cLFV ratios are determined by the Yukawa couplings to the second Higgs doublet, $Y^{(2)}(\omega_{22}, r, \Lambda)$, which also includes neutrino masses and mixings determined by the oscillation parameters. Since the parameter $|\Lambda|$ factors out in the amplitudes as in eq. (3.6), all the relevant parameters for cLFV are ω_{22} , r , $|\Lambda|m_{H^\pm}^2$ and $\Lambda^2 m_{H^\pm}^2$. However, the last one comes from the box diagrams, which is out of the scope of this paper due to a typically negligible box contribution impact for cLFV with relatively light charged Higgs bosons. Neglecting the box contributions, all the relevant free parameters that enter cLFV then sum up to:

$$\omega_{22}, \quad r, \quad |\Lambda|m_{H^\pm}^2. \quad (4.2)$$

The first two are the free parameters that define the Yukawa sector: ω_{22} is a phase that is related to CP and Majorana phases at one-loop, while r parameterizes the mixing between seesaw and radiative states. The last parameter of eq. (4.2) relates the scalar and Yukawa sectors. We will refer to it as the *photon factor*, as it is a factor in front of the amplitudes that include a photon, i.e. in front of A_1^L and A_2^R , as shown in eq. (3.6).

The photon factor, $|\Lambda|m_{H^\pm}^2$, relates the scalar sector to the Yukawa sector via cLFV and it is of most interest. Using eq. (2.19), we write it explicitly:

$$|\Lambda|m_{H^\pm}^2 = \frac{m_4 m_{H^\pm}^2}{32\pi^2} \ln\left(\frac{m_H^2}{m_A^2}\right), \quad m_4 \ll v. \quad (4.3)$$

For the tiny seesaw region, $|\Lambda|m_{H^\pm}^2$ can be generalized to the general 2HDM [42], by inclusion of the mixing of the scalar particles in Λ , eq. (2.19). In our study, we give bounds on the photon factor that are independent of the exact form of the scalar potential or its symmetries (Z_2 or CP breaking or not). Note, however, that the Z_2 symmetry breaking Yukawa couplings of charged leptons to the second Higgs doublet in the Higgs basis can in principle alter the cLFV values, if included.

It is instructive to look at the dependence on the parameters of the scalar potential for the sake of physical intuition. The inert scalar potential of eq. (2.1) in the limit of approximately degenerate heavy scalar masses simplifies the photon factor:⁷

$$|\Lambda|m_{H^\pm}^2 \approx |\lambda_5| m_4 \cdot \frac{v^2}{32\pi^2}. \quad (4.4)$$

⁶See next section.

⁷An exact degeneracy would lead to $\lambda_5 \rightarrow 0$ and vanishing radiative neutrino mass.

Observable	Experiments and constraints
$\mu \rightarrow e\gamma$	MEG [7]: $4.2 \cdot 10^{-13} \rightarrow$ MEG-II [11]: $6 \cdot 10^{-14}$
$\tau \rightarrow e\gamma$	BaBar [8]: $3.3 \cdot 10^{-8} \rightarrow$ Belle-II [12]: $3.0 \cdot 10^{-9}$
$\tau \rightarrow \mu\gamma$	BaBar [8]: $4.5 \cdot 10^{-8} \rightarrow$ Belle-II [12]: $1.0 \cdot 10^{-9}$
$\mu \rightarrow 3e$	SINDRUM [10] : $1 \cdot 10^{-12} \rightarrow$ Mu3e-I [13] : $2 \cdot 10^{-15}$
$\tau \rightarrow 3e$	Belle-I [9]: $2.7 \cdot 10^{-8} \rightarrow$ Belle-II [12]: $4.6 \cdot 10^{-10}$
$\tau \rightarrow \mu ee$	Belle-I [9]: $1.8 \cdot 10^{-8} \rightarrow$ Belle-II [12]: $3.1 \cdot 10^{-10}$
$\tau \rightarrow e\mu\mu$	Belle-I [9]: $2.7 \cdot 10^{-8} \rightarrow$ Belle-II [12]: $4.6 \cdot 10^{-10}$
$\tau \rightarrow 3\mu$	Belle-I [9]: $2.1 \cdot 10^{-8} \rightarrow$ Belle-II [12]: $3.6 \cdot 10^{-10}$
$\mu \rightarrow e$ conversion	$\text{---} \rightarrow$ COMET [14]: $7 \cdot 10^{-15}$

Table 1: Current and planned experimental bounds, related to corresponding observables. Data for τ decays for Belle-II was obtained from the figure 189 of ref. [12]. For the $\mu \rightarrow e$ conversion, we consider the Al nucleus.

The non-observation of cLFV then generally leads to a lower bound on the photon factor $|\Lambda|m_{H^\pm}^2$ (and thus λ_5) as a function of the seesaw scale. As was mentioned before, λ_5 is a Peccei-Quinn symmetry breaking parameter that is bounded from below by the neutrino sector alone. The cLFV decays then allow us to improve this bound in the tiny seesaw region.

As a last note, we stress again that the cLFV rates are related to the scalar sector only via a single parameter, $|\Lambda|m_{H^\pm}^2$. Hence, our results do not depend on how exactly all the parameters in the potential are realized. While we used the scalar potential of the Inert Doublet model (IDM), motivated by an approximate Z_2 symmetry, and assumed that the values of scalar masses are close to each other to get the specific interpretation of a $|\Lambda|m_{H^\pm}^2$ in eq. (4.4), one is, in general, free to use any scenario of the 2HDM potential, as already mentioned before. To construct a consistent potential, one can look at e.g. [65–70] for detailed studies of 2HDM or at [71] for constraints in IDM specifically.

5 Phenomenological analysis

5.1 Discussion of the relative importance of different decay modes

All the cLFV experiments, which potentially can constrain the GNM, are shown in table 1. Below, we discuss the importance of all these decay modes to single out the most constraining experiments for the GNM.

Typically, the branching ratios for three-body decays are dominated by photonic contributions, while others — boxes, Z and Higgs penguins — are negligible in the parameter region defined by eq. (4.1). The tiny seesaw scale, defined as $m_4 \ll v \lesssim m_{H^\pm}$, further leads to a fixed ratio of $A_1^L \approx 2/3A_2^R$. We call this regime *photon* dominance (in contrast to dipole dominance, which assumes $A_1^L \ll A_2^R$):

$$\text{BR}(l_i \rightarrow 3l_j) \approx \left[-\frac{5 \cdot \alpha}{18\pi} + \frac{\alpha}{3\pi} \left(-\frac{11}{4} + \ln \frac{m_i^2}{m_j^2} \right) \right] \cdot \text{BR}(l_i \rightarrow l_j\gamma), \quad (5.1)$$

where $\alpha = e^2/(4\pi)$. The first term of eq. (5.1) is a correction to the dipole dominance. This correction amounts to $O(10\%)$ for $\mu \rightarrow 3e$.

The box contribution can be increased for lower $|\Lambda|$ values, as follows from eq. (3.6). However, two-body decays constrain the $|\Lambda|m_{H^\pm}^2$ factor from below. Taking this minimum value of $|\Lambda|m_{H^\pm}^2$, a lower value for $|\Lambda|$ translates into a higher value for m_{H^\pm} . We concentrate on the lighter masses of the charged Higgs in the paper, see eq. (4.1), where deviations from eq. (5.1) are small.

We find that the box contributions are generally negligible in all of the $\omega_{22} - r$ plane for $\mu \rightarrow 3e$, except for the very small region, where the rate for $\mu \rightarrow e\gamma$ drops sharply close to the point where $Y_\mu^{(2)} = 0$. This is because the constraint on $|\Lambda|m_{H^\pm}^2$ from $\mu \rightarrow e\gamma$ is much looser around that parameter point than in all the rest of the parameter region. Since it is contained in a tiny enough area in the $\omega_{22} - r$ plane and both, $\text{BR}(\mu \rightarrow 3e)$ and $\text{BR}(\mu \rightarrow e\gamma)$ go to zero at $Y_\mu^{(2)} = 0$, it gives negligible modifications to the information that the two-body decays provide.

The only parameter region where $\tau \rightarrow 3\mu$ can be expected to be observed in Belle-II is around $Y_e^{(2)} = 0$; such an observation can happen only if $\tau \rightarrow \mu\gamma$ is also seen. The value of $\tau \rightarrow 3\mu$ can in fact deviate more significantly from photon dominance, but we find that the current and planned experimental sensitivities still leave this process phenomenologically irrelevant. Other three-body processes are not expected to be seen in Belle-II at all. As a result of these checks, we conclude that in the parameter region of our study, the three-body decays are of minor importance compared to the two-body ones.

The second phases of experiments, Mu3e-II and COMET-II, will enhance the importance of the corresponding processes. Their branching ratios will be fixed by the photon dominance contributions in the studied parameter region as box contributions can be neglected. In the present paper, we do not consider these longer-term improvements. For the next achievable improvement of $\mu \rightarrow e$ conversion at COMET [14] the following relation holds:

$$\frac{\text{CR}(\mu \rightarrow e)}{\text{BR}(\mu \rightarrow e\gamma)} < \frac{\text{CR}(\text{COMET})}{\text{BR}(\text{MEG})}, \quad (5.2)$$

which makes it less restrictive than $\mu \rightarrow e\gamma$.

From now on, we will concentrate on the study of two-body decays as the most constraining decay modes for the GNM. Note, however, that two-body decays can vanish if the corresponding Yukawa couplings vanish. These points in the parameter space do exist, as described in section 2.4. Nevertheless, as can be seen from figure 3, there is no such point in the $\omega_{22} - r$ plane in which two of the Yukawa couplings in flavor basis vanish simultaneously. This means that all three two-body decay experiments have to be combined to give a strict bound on $|\Lambda|m_{H^\pm}^2$ and, hence, we further study all three of them.

5.2 Current and planned restrictions on $|\Lambda|m_{H^\pm}^2$

The lower bound for $|\Lambda|m_{H^\pm}^2$ from non-observation of cLFV depends on the parameters r and ω_{22} . The current lower bounds from $\mu \rightarrow e\gamma$ on $|\Lambda|m_{H^\pm}^2$ for NO and IO are given as contour plots in figure 6. The most important observable is $\mu \rightarrow e\gamma$. It gives the tightest bounds almost everywhere, except for the sharp minima around the points, where the

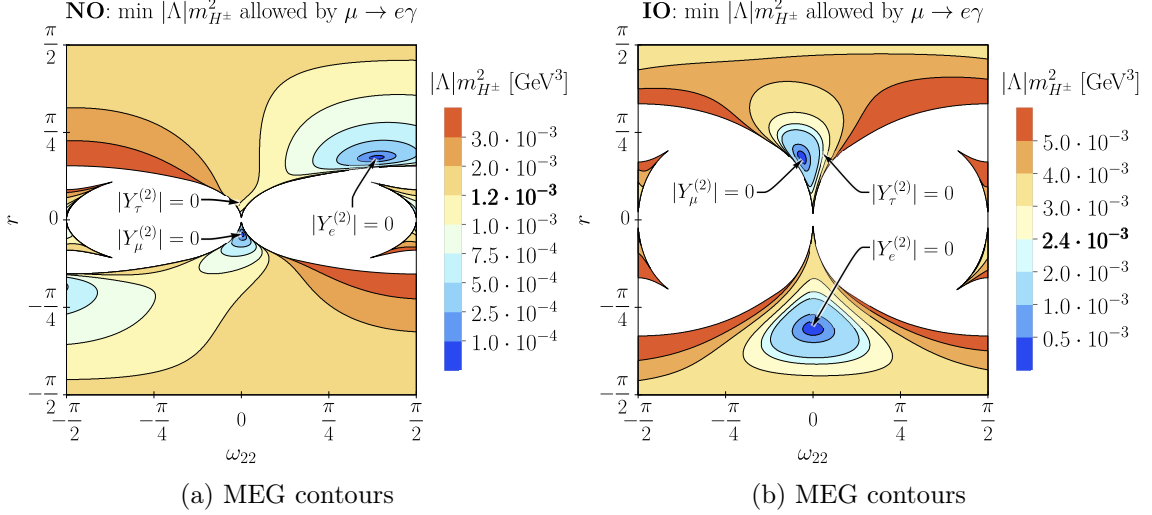


Figure 6: Contour plots of lower limits of $|\Lambda|m_{H^\pm}^2$ for the current bounds on $\mu \rightarrow e\gamma$ by the MEG experiment. The white area is excluded theoretically, either by the constraint that z , eq. (2.26), has to be real, or by the constraint in eq. (2.27). The latter constraint is colored red striped in figure 3. The tiny regions around the points with $Y_e^{(2)} = 0$ and $Y_\mu^{(2)} = 0$ are always allowed by $\mu \rightarrow e\gamma$. They are constrained either by $\tau \rightarrow \mu\gamma$ or $\tau \rightarrow e\gamma$, as in table 2. The bold values of the photon factor correspond to the critical cases when $\mu \rightarrow e\gamma$ allows the point with $Y_\tau^{(2)} = 0$.

Process and parameter point	NO, $ \Lambda m_{H^\pm}^2$ [GeV ³]	IO, $ \Lambda m_{H^\pm}^2$ [GeV ³]
$\tau \rightarrow e\gamma$ at $Y_\mu^{(2)} = 0$	$1.9 \cdot 10^{-6}$	$4.0 \cdot 10^{-6}$
$\tau \rightarrow \mu\gamma$ at $Y_e^{(2)} = 0$	$1.3 \cdot 10^{-5}$	$7.6 \cdot 10^{-6}$

Table 2: Lower bounds on the photon factor, $|\Lambda|m_{H^\pm}^2$, from τ decays at the parameter points, where $\text{BR}(\mu \rightarrow e\gamma)$ vanishes.

corresponding Yukawa couplings vanish. In those small regions, either $\tau \rightarrow e\gamma$ or $\tau \rightarrow \mu\gamma$ constrains the photon factor $|\Lambda|m_{H^\pm}^2$, which results, for the current experimental limits (first column of table 1), in the lower bounds on the photon factor, shown in table 2 (also see figure 8 for current and planned future bounds).

If no cLFV processes are observed in the planned experiments listed in the second column of table 1, one obtains improved bounds on the photon factor $|\Lambda|m_{H^\pm}^2$ by the following scaling:

$$[|\Lambda|m_{H^\pm}^2]_{\text{planned}} = \sqrt{\frac{\text{BR}_i^{\text{current}}}{\text{BR}_i^{\text{planned}}}} [|\Lambda|m_{H^\pm}^2]_{\text{current}}. \quad (5.3)$$

5.3 Some processes are observed: restrictions on the $\omega_{22} - r$ plane

If the planned experiments with improved sensitivity do observe a signal, then the GNM becomes very restrictive. We use table 1 to define regions with respect to the possible

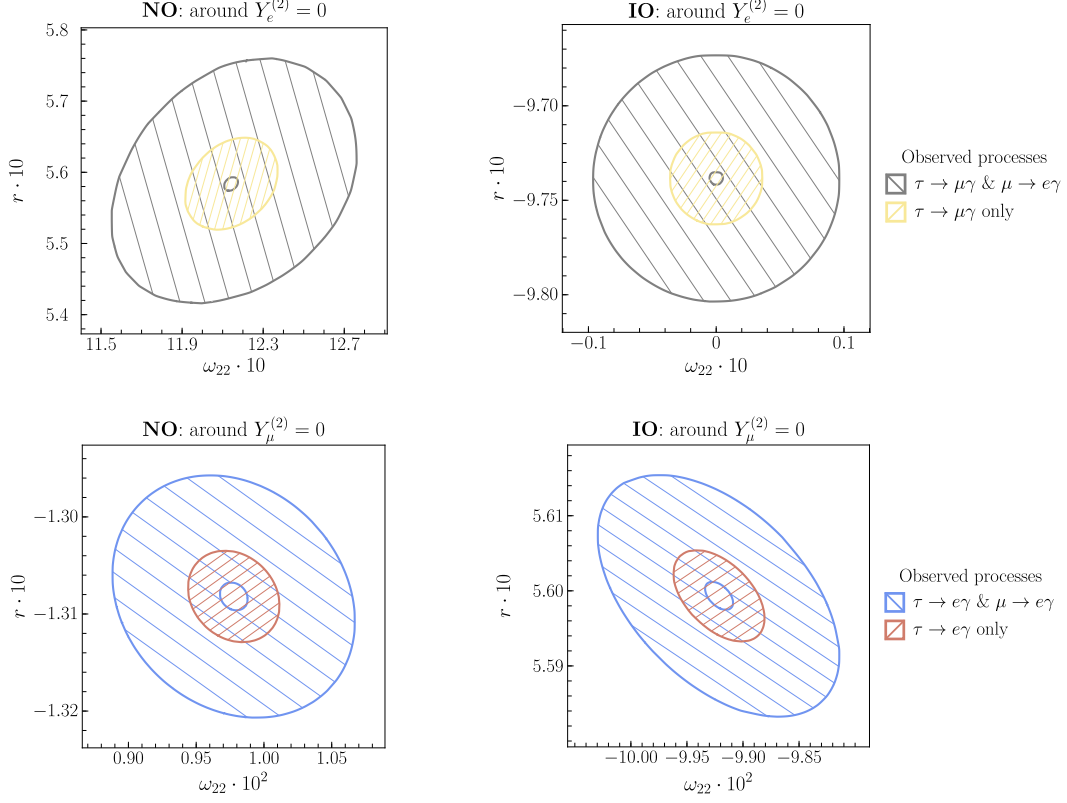


Figure 7: Regions in the $\omega_{22} - r$ plane where the observation of the listed processes is possible in the planned experiments. For example, the gray dashed regions in the upper plots correspond to the case, where $\tau \rightarrow \mu\gamma$ and $\mu \rightarrow e\gamma$ are observed simultaneously, the yellow dashed region shows the allowed values when only $\tau \rightarrow \mu\gamma$ is observed, but $\mu \rightarrow e\gamma$ not, as noted in the plot legend. Note, that the top-left area is significantly larger than other areas.

Observed processes	NO, $ \Lambda m_{H^\pm}^2$ [GeV ³]	IO, $ \Lambda m_{H^\pm}^2$ [GeV ³]
$\tau \rightarrow \mu\gamma$ & $\mu \rightarrow e\gamma$	$9.43 \cdot 10^{-5}$	$5.12 \cdot 10^{-5}$
$\tau \rightarrow \mu\gamma$ only	$9.07 \cdot 10^{-5}$	
$\tau \rightarrow e\gamma$ & $\mu \rightarrow e\gamma$	$6.28 \cdot 10^{-6}$	$1.34 \cdot 10^{-5}$
$\tau \rightarrow e\gamma$ only		

Table 3: Upper bounds on the photon factor, $|\Lambda|m_{H^\pm}^2$, if the only specified combination of processes is observed in Belle-II and MEG-II. Each bound corresponds to a region in the $\omega_{22} - r$ plane in figure 7.

outcomes of the experiments:

$$\text{BR}_i^{\text{planned}} < \text{BR}_i^{\text{observed}} < \text{BR}_i^{\text{current}}, \quad (5.4)$$

where superscripts “current” and “planned” are again used for the reach-in branching ratio of the current or planned experiments. The corresponding values are given in the first and

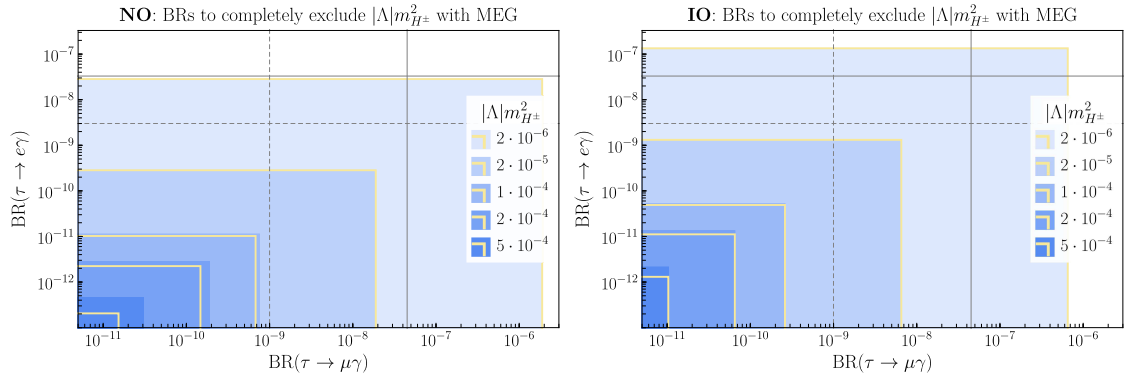


Figure 8: Branching ratios for τ decays within yellow rectangular border allow to exclude the whole $\omega_{22} - r$ plane for a specified photon factor $|\Lambda|m_{H^\pm}^2$ with MEG bounds on $\mu \rightarrow e\gamma$. Closest blue rectangles correspond to the case of infinitely precise experimental bound. To exclude larger photon factor values, bounds on $\mu \rightarrow e\gamma$ have to be improved leading to the same rectangles up to an appropriate scaling of $|\Lambda|m_{H^\pm}^2$ and axes, as mentioned in the text. Gray solid lines correspond to current experimental bounds, gray dashed lines — to the planned ones.

second columns of table 1.

The parameter regions where the observation of $\tau \rightarrow e\gamma$ and $\tau \rightarrow \mu\gamma$ in the $\omega_{22} - r$ plane is possible are shown in figure 7. They also provide the maximal allowed photon factor by the values given in table 3. The lower bounds from table 2 together with the upper ones from table 3 specify the allowed range for the photon factor $|\Lambda|m_{H^\pm}^2$ in case of these observations, while figure 7 shows the allowed regions in the $\omega_{22} - r$ plane: the dashed areas. These dashed areas are disjoint, meaning that the GNM predicts, that $\tau \rightarrow e\gamma$ and $\tau \rightarrow \mu\gamma$ cannot be seen together. If $\mu \rightarrow e\gamma$ is observed, then figure 6, scaled with eq. (5.3) for the observed branching ratio, gives the values of $|\Lambda|m_{H^\pm}^2$ in the $\omega_{22} - r$ plane.

5.4 Nothing is observed: future absolute bounds on $|\Lambda|m_{H^\pm}^2$

To generalize our results and to give a more definite answer of how the combination of the neutrino sector and cLFV constrains the scalar sector, we look at the absolute bound on the photon factor, $|\Lambda|m_{H^\pm}^2$. By absolute bound we mean the minimum value of $|\Lambda|m_{H^\pm}^2$ such that the whole $\omega_{22} - r$ plane, consistent with neutrino masses and mixings, is excluded by cLFV observables. The absolute limits for current experimental bounds are shown in the first row of table 2 and are determined by $\tau \rightarrow e\gamma$ experiments at $Y_\mu^{(2)} = 0$. The limits for the planned experiments are derived with the scaling of eq. (5.3).

In general, $\mu \rightarrow e\gamma$ is the strongest experiment in most of the $\omega_{22} - r$ plane in the nearest future. However, the allowed minimal $|\Lambda|m_{H^\pm}^2$ is mainly determined by the weaker bounds on $\tau \rightarrow e\gamma$ or $\tau \rightarrow \mu\gamma$. This is because one always has two points in the parameter space where $Y_{e,\mu}^{(2)} = 0$ and, hence, the branching ratio for $\mu \rightarrow e\gamma$ vanishes. In order to further improve the absolute bound on $|\Lambda|m_{H^\pm}^2$ one therefore has to improve the experimental sensitivities on $\tau \rightarrow e\gamma$ and $\tau \rightarrow \mu\gamma$. The combination of branching ratios of these exper-

iments, required to completely exclude the $\omega_{22} - r$ plane for specific values of $|\Lambda|m_{H^\pm}^2$, is shown in figure 8.

The yellow borders specify precise values of branching ratios that have to be applied, i.e. if the future $\tau \rightarrow e\gamma$ and $\tau \rightarrow \mu\gamma$ sensitivities are inside one particular yellow rectangle, the absolute lower bound on $|\Lambda|m_{H^\pm}^2$ is at least as good as indicated in the legend. The yellow borders are obtained without approximations and are determined by varying the branching ratio of the τ decays over the regions in the $\omega_{22} - r$ plane that are not excluded by $\mu \rightarrow e\gamma$. The blue rectangles are similar, but they show the hypothetical case in which $\mu \rightarrow e\gamma$ is of infinite precision, and hence only the points with $\text{BR}(\mu \rightarrow e\gamma) = 0$ are allowed by $\mu \rightarrow e\gamma$. All future improvements in $\mu \rightarrow e\gamma$ experiments for a specific value of $|\Lambda|m_{H^\pm}^2$ reside in the area between the closest yellow and blue rectangles. One can see, that the size of the area between the rectangles is small (hence for this analysis improvements in $\mu \rightarrow e\gamma$ are of minor importance) but grows with the values of the photon factor.

This behavior continues to higher values of $|\Lambda|m_{H^\pm}^2$ than shown in the plot, up to the moment when $\mu \rightarrow e\gamma$ allows the point where $Y_\tau^{(2)} = 0$, as shown as critical case in figure 6. To exclude even larger $|\Lambda|m_{H^\pm}^2$ values, the improvement of bounds for $\mu \rightarrow e\gamma$ is required. For a different $\mu \rightarrow e\gamma$ precision, figure 8 can be used with the following rescaling of the photon factor and axes:

$$|\Lambda|m_{H^\pm}^2 \rightarrow |\Lambda|m_{H^\pm}^2 \sqrt{\frac{\text{BR}(\text{MEG})}{\text{BR}(\mu \rightarrow e\gamma)}}, \quad \text{BR}(\tau) \rightarrow \text{BR}(\tau) \frac{\text{BR}(\mu \rightarrow e\gamma)}{\text{BR}(\text{MEG})}. \quad (5.5)$$

However, a high precision of τ experiments is required so that this case lies out of the bounds of figure 8. Taking into account the current and planned bounds for $\tau \rightarrow e\gamma$ and $\tau \rightarrow \mu\gamma$, one concludes that only $\tau \rightarrow e\gamma$ improvements are important for the absolute bound in the near future.

5.5 Interpretation of results: example of limits on λ_5 and relations to scotoseesaw and scotogenic models

The absolute bounds on the photon factor, $|\Lambda|m_{H^\pm}^2$, correspond to the values of the photon factor, for which the entire $\omega_{22} - r$ plane is excluded. They are given by $\tau \rightarrow e\gamma$ in table 2 or figure 8. However, figure 6 shows that the absolute bounds are due to very small areas in the parameter space. These areas are characterized by the vanishing of one of the Yukawa couplings, and only in those regions an observation of τ decays in Belle-II can be expected. We define the “essential part” of the $\omega_{22} - r$ plane, as the region where the observation of τ decays in Belle-II is not possible i.e. all the plane except the regions shown in colors in figure 7. We then obtain a “typical” bound on the photon factor, i.e. the bound for which the “essential part” of the $\omega_{22} - r$ plane is excluded. The absolute bound is shown in table 3 and together with this typical bound, defined above, reads as:

$$\begin{aligned} \text{absolute for NO(IO):} & \quad |\Lambda|m_{H^\pm}^2 > 1.9(4.0) \cdot 10^{-6} \text{ GeV}^3, \\ \text{typical (no } \tau \rightarrow e(\text{or } \mu)\gamma \text{ expected):} & \quad |\Lambda|m_{H^\pm}^2 \gtrsim 10^{-4} \text{ GeV}^3. \end{aligned} \quad (5.6)$$

To get an intuition of how strong this current bound on the scalar sector actually is, we can go back to the special case of the scalar sector, where eq. (4.4) holds. Then eq. (5.6)

translates into bounds on $|\lambda_5|$:

$$\begin{aligned}
\text{absolute for NO(IO):} & \quad |\lambda_5| > 1(2) \cdot 10^{-2} \frac{\text{keV}}{m_4}, \\
\text{typical (no } \tau \rightarrow e(\text{or } \mu)\gamma \text{ expected):} & \quad |\lambda_5| \gtrsim \frac{\text{keV}}{m_4}.
\end{aligned} \tag{5.7}$$

As we mentioned in the introduction, the GNM in the tiny seesaw scale region is similar to the scoto-seesaw and scotogenic models due to an approximate Z_2 symmetry. To put our results in a more general framework let us consider how our results can be applied to these two models.

The scoto-seesaw model has two heavy neutrinos, one of which is odd under the Z_2 symmetry and the other one is even. One can use our parameterization for the Yukawa couplings, where m_4 in $Y^{(2)}$ is understood as the mass of the Z_2 -odd neutrino, while m_4 in the expression for $Y^{(1)}$ has to be understood as the mass of the Z_2 -even neutrino of the scoto-seesaw model. In case these heavy neutrinos of the scoto-seesaw model are lighter than the scalars, only $Y^{(2)}$ enters the cLFV just as in our case, and hence all our results for cLFV, including all figures, hold for the scoto-seesaw model, too. We also note that our parameterization allows to cover the full parameter region of the scoto-seesaw model, while [32, 33] assume only scenarios, where the mixing between the radiative and the seesaw neutrino at one-loop is absent, i.e. $r = 0$ in our parameterization.

The scotogenic model also has a Z_2 symmetry, yet it does have more parameters. Nevertheless, the Casas-Ibarra parameterization gives the same general behavior of the Yukawa couplings with respect to $|\Lambda|m_{H^\pm}^2$ and hence cLFV ratios like in our case. The difference is that in the scotogenic model $|\Lambda|m_{H^\pm}^2$ is a 3×3 matrix and, instead of two parameters, r and ω_{22} , one has a general 3×3 orthogonal matrix entering the Yukawa couplings. Nevertheless, the same *typical* behavior for the tiny seesaw scales in the scotogenic model is to be expected. One should also have in mind that in the scotogenic model there could be similar cancellations suppressing the $\mu \rightarrow e\gamma$ branching ratio like in our case. These cancellations would push the absolute bound on $|\Lambda|m_{H^\pm}^2$ lower. However, from our study we cannot generalize our strict exclusions and predict them for the scotogenic model.

Even though the tiny seesaw scale has never been rigorously studied in the scotogenic model before, we do find the comment about it in [30], which gives us some way to put our results in a more general context. [30] claims that for $m_4 \ll m_{H^\pm}$ the value $\lambda_5 = 10^{-9}$ is excluded. We see that the typical bound, given in eq. (5.7), indeed is consistent with this statement for scalar masses of the TeV scale, which are the masses they actually consider. This confirms our expectation that the typical behavior of the models in this parameter region is the same. As said before, our absolute bound from eq. (5.7) cannot be directly applied to the scotogenic model, yet it gives an example of how much special analytical solutions, that can hardly be caught in random parameter scans, can push the strict exclusion limits of the model.

6 Conclusions

Throughout this paper, we concentrated on the question: how does the neutrino sector of the GNM constrain the scalar sector via cLFV observables? The GNM is a model where neutrino masses are generated with a minimal neutrino sector but a non-minimal Higgs sector, such that new Yukawa couplings can lead to cLFV effects. Guided by the principle “exclude as much as possible”, we singled out the scenario where the strongest constraints can be drawn, i.e. when cLFV decays are enhanced. This scenario corresponds to a tiny seesaw scale (lower than the electroweak scale) and a mass of the charged Higgs m_{H^\pm} slightly above the electroweak scale (up to a TeV).

In this parameter range, box diagrams are negligible, and the study simplifies to the relations between three parameters: two parameters, ω_{22} and r , parameterize the new Yukawa sector, see figure 3, and one parameter, the so-called photon factor $|\Lambda|m_{H^\pm}^2$, includes scalar sector parameters and the seesaw scale, see eq. (4.3).

The non-observation of cLFV then results in lower bounds on the photon factor as a function of ω_{22} and r . These lower bounds are shown as contour plots in figure 6 for each neutrino mass ordering. Currently, $\mu \rightarrow e\gamma$ is the most constraining observable in the largest part of the $\omega_{22} - r$ plane. There are only two areas in this plane where $\mu \rightarrow e\gamma$ gives weaker constraints than $\tau \rightarrow e\gamma$ and $\tau \rightarrow \mu\gamma$, corresponding to areas of approximately zero Yukawa couplings $Y_e^{(2)}, Y_\mu^{(2)} = 0$. Hence, the final, absolute constraints on the photon factor $|\Lambda|m_{H^\pm}^2$ (which are independent of ω_{22} and r) come from τ decays and are given separately in table 2.

In the mentioned special parameter areas, the observation of $\tau \rightarrow e\gamma$ or $\tau \rightarrow \mu\gamma$ in the planned experiments becomes possible and leads to the regions shown in figure 7. The upper limits on $|\Lambda|m_{H^\pm}^2$ for these decays is given in table 3. Hence, if $\tau \rightarrow e\gamma$ or $\tau \rightarrow \mu\gamma$ is observed in the future, the parameter space is drastically reduced, while the observation of both $\tau \rightarrow e\gamma$ and $\tau \rightarrow \mu\gamma$ is excluded in the GNM by the sensitivity of $\mu \rightarrow e\gamma$.

To disentangle the discussion of the neutrino sector and the scalar sector, we look at global bounds on $|\Lambda|m_{H^\pm}^2$, which are independent of the neutrino parameters ω_{22} and r . One option is to consider *absolute* bounds, i.e. bounds for which the complete $\omega_{22} - r$ plane is strictly excluded. To increase this absolute bound an improvement of the sensitivity in $\tau \rightarrow e\gamma$ is most important in the near future. This situation is shown in figure 8, where the needed branching ratios of $\tau \rightarrow e\gamma$ and $\tau \rightarrow \mu\gamma$ to exclude the particular value of $|\Lambda|m_{H^\pm}^2$ for the complete parameter space of the model can be extracted. For instance, until the $\text{BR}(\tau \rightarrow e\gamma) \approx 10^{-11}(10^{-10})$ for NO(IO) is probed, any other improvement of cLFV observables has no effect on the bound on the photon factor $|\Lambda|m_{H^\pm}^2$. Technically, the absolute bound is driven by the point, where $Y_\mu^{(2)} = 0$, see table 2. In the numerical evaluation it is helpful to rely on analytical solutions for such points, provided in section 2.4.

A second option is to consider *typical* bounds, i.e. bounds on $|\Lambda|m_{H^\pm}^2$ for which the essential part of the $\omega_{22} - r$ plane is excluded. The absolute and typical bounds are shown in eq. (5.6) and interpreted in terms of the scalar sector parameter λ_5 in eq. (5.7).

All the presented results are directly applicable to the scoto-seesaw model and complement the current studies of [32, 33]. Additionally, the presented neutrino mass calculation

and the parameterization of the Yukawa couplings are more accurate and do not neglect the mixing between the radiative and the seesaw neutrino states at one loop as in [32, 33]. This allows us to cover the parameter space completely.

One cannot apply the absolute bound from the GNM directly to the scotogenic model. In both models, the dependence on the photon factor coincides, but there are more free parameters in the Yukawa sector of the scotogenic model. This leads to unrelated analytical solutions in the limiting case. However, as discussed in section 5.5, the typical bounds of eqs. (5.6, 5.7) are applicable for the typical behavior of the scotogenic model.

Acknowledgments

W.K. was supported in part by the German Research Foundation (DFG) under grant number STO 876/2-2 and by the National Science Centre (Poland) under the research grant 2020/38/E/ST2/00126. U.Kh. was supported by the Deutscher Akademischer Austauschdienst (DAAD) under Research Grants — Doctoral Programmes in Germany, 2019/20 (57440921) and by the DFG under grant number STO 876/7-1. This project has received funding from the European Social Fund (project No 09.3.3-LMT-K-712-19-0013) under the grant agreement with the Research Council of Lithuania (LMTLT).

A Parametrization for Yukawa couplings

In this appendix we give the step by step derivation of how we can define the Yukawa couplings unambiguously.

We start with defining the loop contribution to $\hat{\Sigma}$, eq. (2.19), as

$$W := -\Lambda \hat{R}^* \begin{pmatrix} d^2 & idd' \\ idd' & -d'^2 \end{pmatrix} \hat{R}^\dagger = \hat{R}^* \begin{pmatrix} 0 & 0 \\ 0 & m_3 \end{pmatrix} \hat{R}^\dagger - \text{diag}(m_2^{\text{pole}}, m_3^{\text{pole}}), \quad (\text{A.1})$$

which has determinant zero. For convenience we repeat the definition of \hat{R} :

$$\hat{R} = \begin{pmatrix} R_{22} & -R_{32}^* e^{i\phi_R} \\ R_{32} & R_{22}^* e^{i\phi_R} \end{pmatrix}, \quad \text{with} \quad R_{22} := \cos r e^{i\omega_{22}}, \quad R_{32} := \sin r e^{i\omega_{32}}. \quad (\text{A.2})$$

Defining

$$z := R_{22}^2 + t_{32} R_{32}^2 \quad \text{and} \quad t_{32} := \frac{m_3^{\text{pole}}}{m_2^{\text{pole}}}, \quad (\text{A.3})$$

we can restrict the components of \hat{R} by the condition, that the determinant of the rhs. of eq. (A.1) vanishes:

$$\begin{aligned} 0 = \det W &= m_2^{\text{pole}} m_3^{\text{pole}} - e^{-2i\phi_R} m_3 (m_2^{\text{pole}} R_{22}^2 + m_3^{\text{pole}} R_{32}^2) \\ &= m_2^{\text{pole}} [m_3^{\text{pole}} - e^{-2i\phi_R} m_3 (R_{22}^2 + t_{32} R_{32}^2)] = m_2^{\text{pole}} [m_3^{\text{pole}} - e^{-2i\phi_R} m_3 z], \end{aligned} \quad (\text{A.4})$$

giving us a definition of the phase ϕ_R :

$$\frac{e^{2i\phi_R}}{z} = \frac{m_3}{m_3^{\text{pole}}} > 0. \quad (\text{A.5})$$

W itself, eq. (A.1), produces also additional relations between d , d' and \hat{R}_{ij} :

$$[-\hat{R}^T W \hat{R}]_{11} = d^2 \Lambda = m_2^{\text{pole}} R_{22}^2 + m_3^{\text{pole}} R_{32}^2 = m_2^{\text{pole}} z. \quad (\text{A.6})$$

Since Λ is real, see eq. (2.19), we get from eq. (A.6)

$$\Lambda/z = m_2^{\text{pole}}/d^2 > 0, \quad \text{Im } z = 0, \quad (\text{A.7})$$

meaning that z has to be real, and additionally, has to have the same sign as Λ . From eq. (A.5) we get then

$$e^{2i\phi_R} = \text{sign}(z) = \text{sign}(\Lambda), \quad (\text{A.8})$$

which allows two values for $e^{i\phi_R}$, depending on the sign of Λ :

$$e^{i\phi_R} = \pm \sqrt{\text{sign}(\Lambda)} \quad \text{or equivalently} \quad e^{i\phi_R}|_{\Lambda>0} = \pm 1 \quad \text{or} \quad e^{i\phi_R}|_{\Lambda<0} = \pm i. \quad (\text{A.9})$$

From our limit on the range of m_3 , eq. (2.24), we get also a limit for $|z| = m_3^{\text{pole}}/m_3$:

$$\frac{1}{2} < |z| \leq t_{32}. \quad (\text{A.10})$$

Using above definitions and conditions, eqs. (A.3, A.5), it turns out that we can rewrite

$$\begin{aligned} W_{rhs.} &= \begin{pmatrix} -m_2^{\text{pole}} + e^{-2i\phi_R} m_3 R_{32}^2 & -e^{-2i\phi_R} m_3 R_{22} R_{32} \\ -e^{-2i\phi_R} m_3 R_{22} R_{32} & -m_3^{\text{pole}} + e^{-2i\phi_R} m_3 R_{22}^2 \end{pmatrix} \\ &= \begin{pmatrix} -m_2^{\text{pole}} + \frac{t_{32} m_2^{\text{pole}}}{z m_3} m_3 R_{32}^2 & -\frac{t_{32} m_2^{\text{pole}}}{z m_3} m_3 R_{22} R_{32} \\ -\frac{t_{32} m_2^{\text{pole}}}{z m_3} m_3 R_{22} R_{32} & -t_{32} m_2^{\text{pole}} + \frac{t_{32} m_2^{\text{pole}}}{z m_3} m_3 R_{22}^2 \end{pmatrix} \\ &= -\frac{m_2^{\text{pole}}}{z} \begin{pmatrix} z - t_{32} R_{32}^2 & t_{32} R_{22} R_{32} \\ t_{32} R_{22} R_{32} & z t_{32} - t_{32} R_{22}^2 \end{pmatrix} \\ &= -\frac{m_2^{\text{pole}}}{z} \begin{pmatrix} R_{22}^2 + t_{32} R_{32}^2 - t_{32} R_{32}^2 & t_{32} R_{22} R_{32} \\ t_{32} R_{22} R_{32} & t_{32} (R_{22}^2 + t_{32} R_{32}^2 - R_{22}^2) \end{pmatrix} \\ &= -\frac{m_2^{\text{pole}}}{z} \begin{pmatrix} R_{22}^2 & t_{32} R_{22} R_{32} \\ t_{32} R_{22} R_{32} & t_{32}^2 R_{32}^2 \end{pmatrix} \end{aligned} \quad (\text{A.11})$$

as a tensor product:

$$W_{rhs.} = -\frac{m_2^{\text{pole}}}{z} w \otimes w, \quad w := \begin{pmatrix} R_{22} \\ t_{32} R_{32} \end{pmatrix}. \quad (\text{A.12})$$

Motivated by this decomposition we can extend the tensor product definition, using eq. (2.10), and \hat{R} from eq. (2.9) to express:

$$Y^{(2\mu)} \otimes Y^{(2\nu)} = \begin{pmatrix} 0 & 0 \\ 0 & -\frac{1}{\Lambda} W_{lhs.} \end{pmatrix} = \begin{pmatrix} 0 & 0 \\ 0 & -\frac{1}{\Lambda} W_{rhs.} \end{pmatrix} = \begin{pmatrix} 0 & 0 \\ 0 & \frac{m_2^{\text{pole}}}{z \Lambda} w \otimes w \end{pmatrix}. \quad (\text{A.13})$$

This expression motivates a parameterization for the Yukawa coupling $Y^{(2\mu)}$,

$$Y^{(2\mu)} = \text{sign}(\Lambda) \sqrt{\frac{m_2^{\text{pole}}}{z \Lambda}} (0, R_{22}, t_{32} R_{32}) = Y^{(2\prime)} R^\dagger = (0, d, id') R^\dagger, \quad (\text{A.14})$$

or

$$d = \text{sign}(\Lambda) \sqrt{\frac{m_2^{\text{pole}}}{z\Lambda}} (R_{22}^2 + t_{32}R_{32}^2) = \frac{\Lambda}{|\Lambda|} \sqrt{\frac{m_2^{\text{pole}}}{z\Lambda}} z = \frac{\sqrt{m_2^{\text{pole}} z\Lambda}}{|\Lambda|} > 0, \quad (\text{A.15})$$

$$id' = \text{sign}(\Lambda) \sqrt{\frac{m_2^{\text{pole}}}{z\Lambda}} (-R_{22}R_{32}^* + t_{32}R_{32}R_{22}^*) e^{i\phi_R},$$

which is consistent with the $[-\hat{R}^T W \hat{R}]_{12}$ element of eq. (A.1)

$$\begin{aligned} idd'\Lambda &= e^{i\phi_R} (m_3^{\text{pole}} R_{32} R_{22}^* - m_2^{\text{pole}} R_{22} R_{32}^*) \\ &= m_2^{\text{pole}} e^{i\phi_R} (t_{32} R_{32} R_{22}^* - R_{22} R_{32}^*) \\ &= m_2^{\text{pole}} \sin r \cos r e^{i\phi_R} (t_{32} e^{i(\omega_{32} - \omega_{22})} - e^{-i(\omega_{32} - \omega_{22})}). \end{aligned} \quad (\text{A.16})$$

Analogously, we have to rotate the Yukawa coupling to the first Higgs doublet:

$$Y^{(1'')} = Y^{(1')} R^\dagger = (0, 0, iy) R^\dagger = ie^{-i\phi_R} \sqrt{\frac{2m_3^{\text{pole}} m_4}{|z|v^2}} (0, -R_{32}, R_{22}), \quad (\text{A.17})$$

using eq. (2.6, A.5).

B Determining the minimal parameter space

In this appendix we derive a minimal region of ϕ_R , r , ω_{22} , and ω_{32} that covers the whole parameter space to study the unique constraints by cLFV. The dominant contribution of all cLFV processes in our region of interest, that is motivated by the approximate Z_2 symmetry, depends on $Y_i^{(2)} Y_j^{(2)*}$, which implies, that parameter points leading to a different overall *phase* of $Y^{(2)}$ are equivalent.

With the new definitions for $Y^{(n)}$ from eq. (A.14)

$$Y^{(2'')} = \text{sign}(\Lambda) \sqrt{\frac{m_2^{\text{pole}}}{z\Lambda}} (0, R_{22}, t_{32}R_{32}) = \text{sign}(\Lambda) \sqrt{\frac{m_2^{\text{pole}}}{z\Lambda}} (0, \cos r e^{i\omega_{22}}, t_{32} \sin r e^{i\omega_{32}}),$$

and eq. (A.17)

$$Y^{(1'')} = Y^{(1')} R^\dagger = (0, 0, iy) R^\dagger = ie^{-i\phi_R} \sqrt{\frac{2m_3^{\text{pole}} m_4}{|z|v^2}} (0, -\sin r e^{i\omega_{32}}, \cos r e^{i\omega_{22}}),$$

we see the following relation

$$Y^{(n)}(r \pm \pi) = -Y^{(n)}(r) \quad \Rightarrow \quad r \in \left(-\frac{\pi}{2}, \frac{\pi}{2}\right], \quad (\text{B.1})$$

that reduces the required region of r , as the minus signs are just a different phase, that does not influence the cLFV. In the same way, we can pick in eq. (A.9) the plus sign before the square root, as the different phase does not influence the cLFV.

The restrictions for r and ω_{22} come from solving eq. (A.7) for ω_{32} :

$$\begin{aligned} 0 = \text{Im } z = \text{Im}[R_{22}^2 + t_{32}R_{32}^2] &= \cos^2 r \sin(2\omega_{22}) + t_{32} \sin^2 r \sin(2\omega_{32}) \\ &= \cos^2 r \sin(2\omega_{22}) + t_{32} \sin^2 r \frac{1}{2i}[e^{2i\omega_{32}} - e^{-2i\omega_{32}}] \end{aligned} \quad (\text{B.2})$$

gives two possible distinct solutions for ω_{32} as functions of ω_{22} , as $e^{i\omega_{32}}$ is needed for the Yukawas, but the equation determines only the square, $e^{2i\omega_{32}}$:

$$0 = e^{2i\omega_{32}} + 2i \frac{\sin(2\omega_{22})}{t_{32} \tan^2 r} - e^{-2i\omega_{32}}, \quad (\text{B.3})$$

or

$$(e^{2i\omega_{32}})_{1,2} = -i \frac{\sin(2\omega_{22})}{t_{32} \tan^2 r} \pm \sqrt{1 - \frac{\sin^2(2\omega_{22})}{t_{32}^2 \tan^4 r}}, \quad (\text{B.4})$$

giving immediately

$$[\sin(2\omega_{32})]_1 = [\sin(2\omega_{32})]_2 = -\frac{\sin(2\omega_{22})}{t_{32} \tan^2 r} \quad (\text{B.5})$$

and

$$[\cos(2\omega_{32})]_{1,2} = \pm \sqrt{1 - \frac{\sin^2(2\omega_{22})}{t_{32}^2 \tan^4 r}}. \quad (\text{B.6})$$

One can directly see, that $(e^{2i\omega_{32}})_2 = [-(e^{2i\omega_{32}})_1]^{-1}$. Additionally, eqs. (B.5, B.6) restrict r and ω_{22} by

$$t_{32} \tan^2 r > |\sin(2\omega_{22})|, \quad (\text{B.7})$$

which is displayed as the white “disks” in figure 3. In these white “disks” there exists no solution to consistency conditions imposed by eq. (A.1).

We take as the regular solution, inspired by eq. (B.5):

$$\omega_{32+} := -\frac{1}{2} \arcsin\left(\frac{\sin(2\omega_{22})}{t_{32} \tan^2 r}\right), \quad \omega_{32+}(r=0) := 0, \quad (\text{B.8})$$

which lies by construction in the range $|\omega_{32}| < \pi/4$, giving $\cos(2\omega_{32}) \geq 0$. To reach the second choice, $\cos(2\omega_{32}) < 0$, we take:

$$\omega_{32-} := -\frac{\pi}{2} \text{sign}(\omega_{22}) - \omega_{32+}. \quad (\text{B.9})$$

Both ω_{32+} and ω_{32-} lead to regions with positive and negative values for z :

$$\begin{aligned} z_+ &:= \text{Re}[z(\omega_{32+})] = \text{Re}[R_{22}^2 + t_{32}R_{32}^2] = \cos^2 r \cos(2\omega_{22}) + t_{32} \sin^2 r \cos(2\omega_{32+}) \\ &= \cos^2 r \left[\cos(2\omega_{22}) + t_{32} \tan^2 r \sqrt{1 - \frac{\sin^2(2\omega_{22})}{t_{32}^2 \tan^4 r}} \right]. \end{aligned} \quad (\text{B.10})$$

If

$$\begin{aligned} &t_{32}^2 \tan^4 r \left[1 - \frac{\sin^2(2\omega_{22})}{t_{32}^2 \tan^4 r} \right] \geq \cos^2(2\omega_{22}) \\ \Leftrightarrow &t_{32}^2 \tan^4 r \geq \cos^2(2\omega_{22}) + t_{32}^2 \tan^4 r \frac{\sin^2(2\omega_{22})}{t_{32}^2 \tan^4 r} = 1 \\ \Leftrightarrow &t_{32} \tan^2 r \geq 1, \end{aligned} \quad (\text{B.11})$$

$z_+ > 0$ for any value of ω_{22} . But if

$$t_{32} \tan^2 r \leq 1 \quad (\text{B.12})$$

z_+ can become negative for $|\omega_{22}| > \frac{\pi}{4}$.

A similar distinction happens to

$$\begin{aligned} z_- &:= \text{Re}[z(\omega_{32-})] = \text{Re}[R_{22}^2 + t_{32}R_{32}^2] = \cos^2 r \cos(2\omega_{22}) + t_{32} \sin^2 r \cos(2\omega_{32-}) \\ &= \cos^2 r \cos(2\omega_{22}) + t_{32} \sin^2 r \cos(\mp\pi - 2\omega_{32+}) \\ &= \cos^2 r \cos(2\omega_{22}) - t_{32} \sin^2 r \cos(-2\omega_{32+}) \\ &= \cos^2 r \left[\cos(2\omega_{22}) - t_{32} \tan^2 r \sqrt{1 - \frac{\sin^2(2\omega_{22})}{t_{32}^2 \tan^4 r}} \right]. \end{aligned} \quad (\text{B.13})$$

For eq. (B.11) the negative term always dominates and $z_- \leq 0$ for any ω_{22} . But if eq. (B.12), the first term dominates and $z_- \geq 0$ if $|\omega_{22}| < \frac{\pi}{4}$.

Since z and Λ have the same sign, eq. (A.7), the sign of Λ determines also, how the choice of ω_{22} , effects the possible solutions of eq. (A.7) or eq. (B.2), i.e. ω_{32+} or ω_{32-} , as the sign of z is an additional requirement for the solution:

- in the case of a positive sign of Λ , we have to choose also a positive sign for z :
 - z_+ in the region eq. (B.11) and the region eq. (B.12) and $|\omega_{22}| < \frac{\pi}{4}$
 - z_- in the region eq. (B.12) and $|\omega_{22}| > \frac{\pi}{4}$
- in the case of a negative sign of Λ , we have to choose a negative sign for z :
 - z_+ in the region eq. (B.12) and $|\omega_{22}| > \frac{\pi}{4}$
 - z_- in the region eq. (B.11) and the region eq. (B.12) and $|\omega_{22}| < \frac{\pi}{4}$

Summarizing, we get the possible Yukawa couplings:

$$Y^{(\prime\prime)}(\Lambda, t_{32} \tan^2 r < |\sin(2\omega_{22})|) \quad := \text{not defined} \quad (\text{B.14})$$

$$Y^{(\prime\prime)}(\Lambda > 0, t_{32} > \cot^2 r) \quad := Y^{(\prime\prime)}(r, \omega_{22}; \omega_{32+}) \quad (\text{B.15})$$

$$Y^{(\prime\prime)}(\Lambda > 0, t_{32} < \cot^2 r, |\omega_{22}| < \pi/4) \quad := Y^{(\prime\prime)}(r, \omega_{22}; \omega_{32+}) \quad (\text{B.16})$$

$$Y^{(\prime\prime)}(\Lambda > 0, t_{32} < \cot^2 r, |\omega_{22}| > \pi/4) \quad := Y^{(\prime\prime)}(r, \omega_{22}; \omega_{32-}) \quad (\text{B.17})$$

$$Y^{(\prime\prime)}(\Lambda < 0, t_{32} < \cot^2 r, |\omega_{22}| > \pi/4) \quad := Y^{(\prime\prime)}(r, \omega_{22}; \omega_{32+}) \quad (\text{B.18})$$

$$Y^{(\prime\prime)}(\Lambda < 0, t_{32} > \cot^2 r) \quad := Y^{(\prime\prime)}(r, \omega_{22}; \omega_{32-}) \quad (\text{B.19})$$

$$Y^{(\prime\prime)}(\Lambda < 0, t_{32} < \cot^2 r, |\omega_{22}| < \pi/4) \quad := Y^{(\prime\prime)}(r, \omega_{22}; \omega_{32-}). \quad (\text{B.20})$$

We see, that the areas where one has to use the ‘‘other’’ solution, i.e. ω_{32-} instead of ω_{32+} , or $\Lambda > 0$ compared to $\Lambda < 0$, are complementary: we cover the whole parameter space in all cases.

C Relations between Yukawa couplings of different parameter points

It turns out, that there is a relation between the parameters of \hat{R} , that gives the same Yukawa couplings for both solutions, ω_{32+} and ω_{32-} . We also notice that the conditions for the allowed areas in the $\omega_{22} - r$ plane depend only on the sizes of $|r|$ and $|\omega_{22}|$.

The first observation needed is the relation between $\omega_{32+}[\omega_{22}]$, eq. (B.8), and $\omega_{32-}[\widetilde{\omega}_{22}]$, eq. (B.9), for a shifted $\widetilde{\omega}_{22} = \omega_{22} - \frac{\pi}{2}\text{sign}(\omega_{22})$. Please note, that this shift flips between the regions $|\omega_{22}| < \frac{\pi}{4}$ and $|\omega_{22}| > \frac{\pi}{4}$.

$$\begin{aligned}
\omega_{32-}[\widetilde{\omega}_{22}] &= \omega_{32-}[\omega_{22} - \frac{\pi}{2}\text{sign}(\omega_{22})] \\
&= -\frac{\pi}{2}\text{sign}(\omega_{22}) + \frac{1}{2}\arcsin\left(\frac{\sin(2[\omega_{22} - \frac{\pi}{2}\text{sign}(\omega_{22})])}{t_{32}\tan^2 r}\right) \\
&= -\frac{\pi}{2}\text{sign}(\omega_{22}) + \frac{1}{2}\arcsin\left(\frac{\sin(2\omega_{22} \mp \pi)}{t_{32}\tan^2 r}\right) \\
&= -\frac{\pi}{2}\text{sign}(\omega_{22}) + \frac{1}{2}\arcsin\left(\frac{-\sin(2\omega_{22})}{t_{32}\tan^2 r}\right) \\
&= -\frac{\pi}{2}\text{sign}(\omega_{22}) - \frac{1}{2}\arcsin\left(\frac{\sin(2\omega_{22})}{t_{32}\tan^2 r}\right) \\
&= -\frac{\pi}{2}\text{sign}(\omega_{22}) + \omega_{32+}[\omega_{22}].
\end{aligned} \tag{C.1}$$

The second relation is the one between $z_-(\widetilde{\omega}_{22})$, eq. (B.13), and $z_+(\omega_{22})$, eq. (B.10):

$$\begin{aligned}
z_- &= \cos^2 r \cos(2\widetilde{\omega}_{22}) + t_{32}\sin^2 r \cos(2\omega_{32-}[\widetilde{\omega}_{22}]) \\
&= \cos^2 r \cos(2[\omega_{22} - \frac{\pi}{2}\text{sign}(\omega_{22})]) + t_{32}\sin^2 r \cos(2[\omega_{32+}[\omega_{22}] - \frac{\pi}{2}\text{sign}(\omega_{22})]) \\
&= \cos^2 r \cos(2\omega_{22} \mp \pi) + t_{32}\sin^2 r \cos(2\omega_{32+}[\omega_{22}] \mp \pi) \\
&= -\cos^2 r \cos(2\omega_{22}) - t_{32}\sin^2 r \cos(2\omega_{32+}[\omega_{22}]) = -z_+(\omega_{22}).
\end{aligned} \tag{C.2}$$

With $\text{sign}(\Lambda) = \text{sign}(z) = +1$ this gives now

$$\begin{aligned}
Y^{(1\prime\prime)}(\Lambda > 0, t_{32} < \cot^2 r, |\widetilde{\omega}_{22}| > \pi/4) &= Y^{(1\prime\prime)}(r, \widetilde{\omega}_{22}; \omega_{32-}[\widetilde{\omega}_{22}]) \\
&= i\sqrt{\text{sign}(z_-)}\sqrt{\frac{2m_3^{\text{pole}}m_4}{|z_-[\widetilde{\omega}_{22}]|v^2}}(0, -\sin r e^{i\omega_{32-}[\widetilde{\omega}_{22}]}, \cos r e^{i\widetilde{\omega}_{22}}) \\
&= i\sqrt{\text{sign}(-z_+)}\sqrt{\frac{2m_3^{\text{pole}}m_4}{|-z_+[\omega_{22}]|v^2}}(0, -\sin r e^{i\omega_{32+}[\omega_{22}] - \frac{i\pi}{2}\text{sign}(\omega_{22})}, \cos r e^{i\omega_{22} - \frac{i\pi}{2}\text{sign}(\omega_{22})}) \\
&= i\sqrt{-\text{sign}(z_+)}e^{-\frac{i\pi}{2}\text{sign}(\omega_{22})}\sqrt{\frac{2m_3^{\text{pole}}m_4}{|z_+[\omega_{22}]|v^2}}(0, -\sin r e^{i\omega_{32+}[\omega_{22}]}, \cos r e^{i\omega_{22}}) \\
&= \sqrt{-e^{-i\pi\text{sign}(\omega_{22})}}Y^{(1\prime\prime)}(r, \omega_{22}; \omega_{32+}[\omega_{22}]) \\
&= Y^{(1\prime\prime)}(r, \omega_{22}; \omega_{32+}[\omega_{22}]) = Y^{(1\prime\prime)}(\Lambda > 0, t_{32} < \cot^2 r, |\omega_{22}| < \pi/4),
\end{aligned} \tag{C.3}$$

or with $\text{sign}(\Lambda) = \text{sign}(z) = -1$ we get

$$\begin{aligned}
Y^{(1')}(\Lambda < 0, t_{32} < \cot^2 r, |\widetilde{\omega}_{22}| < \pi/4) &= Y^{(1')}(r, \widetilde{\omega}_{22}; \omega_{32-}[\widetilde{\omega}_{22}]) \\
&= i\sqrt{\text{sign}(z_-)} \sqrt{\frac{2m_3^{\text{pole}} m_4}{|z_-[\widetilde{\omega}_{22}]|^2}} (0, -\sin r e^{i\omega_{32-}[\widetilde{\omega}_{22}]}, \cos r e^{i\widetilde{\omega}_{22}}) \\
&= i\sqrt{\text{sign}(-z_+)} \sqrt{\frac{2m_3^{\text{pole}} m_4}{|-z_+[\omega_{22}]|^2}} (0, -\sin r e^{i\omega_{32+}[\omega_{22}] - \frac{i\pi}{2}\text{sign}(\omega_{22})}, \cos r e^{i\omega_{22} - \frac{i\pi}{2}\text{sign}(\omega_{22})}) \\
&= i\sqrt{-\text{sign}(z_+)} e^{-\frac{i\pi}{2}\text{sign}(\omega_{22})} \sqrt{\frac{2m_3^{\text{pole}} m_4}{|z_+[\omega_{22}]|^2}} (0, -\sin r e^{i\omega_{32+}[\omega_{22}]}, \cos r e^{i\omega_{22}}) \\
&= \sqrt{-e^{-i\pi\text{sign}(\omega_{22})}} Y^{(1')}(r, \omega_{22}; \omega_{32+}[\omega_{22}]) \\
&= Y^{(1')}(r, \omega_{22}; \omega_{32+}[\omega_{22}]) = Y^{(1')}(\Lambda < 0, t_{32} < \cot^2 r, |\omega_{22}| > \pi/4),
\end{aligned} \tag{C.4}$$

but now for the opposite sign of Λ .

In the same way we get for any sign of Λ

$$\begin{aligned}
Y^{(2'')}(r, \widetilde{\omega}_{22}; \omega_{32-}[\widetilde{\omega}_{22}]) \\
&= \text{sign}(\Lambda) \sqrt{\frac{m_2^{\text{pole}}}{z_-[\widetilde{\omega}_{22}]\Lambda}} (0, \cos r e^{i\widetilde{\omega}_{22}}, t_{32} \sin r e^{i\omega_{32-}[\widetilde{\omega}_{22}]}) \\
&= \text{sign}(\Lambda) \sqrt{\frac{m_2^{\text{pole}}}{-z_+[\omega_{22}]\Lambda}} (0, \cos r e^{i\omega_{22} - \frac{i\pi}{2}\text{sign}(\omega_{22})}, t_{32} \sin r e^{i\omega_{32+}[\omega_{22}] - \frac{i\pi}{2}\text{sign}(\omega_{22})}) \\
&= \text{sign}(\Lambda) e^{-\frac{i\pi}{2}\text{sign}(\omega_{22})} \sqrt{-1} \sqrt{\frac{m_2^{\text{pole}}}{z_+[\omega_{22}]\Lambda}} (0, \cos r e^{i\omega_{22}}, t_{32} \sin r e^{i\omega_{32+}[\omega_{22}]}) \\
&= \sqrt{-e^{-i\pi\text{sign}(\omega_{22})}} Y^{(2'')}(r, \omega_{22}; \omega_{32+}[\omega_{22}]) = Y^{(2'')}(r, \omega_{22}; \omega_{32+}[\omega_{22}]),
\end{aligned} \tag{C.5}$$

which allows us to cover all values of Yukawa couplings with sweeping over the $\omega_{22} - r$ plane with only using ω_{32+} for the definition of the Yukawa couplings, as done in eqs. (2.30, 2.29).

D Numerical values for Yukawas on the $\omega_{22} - r$ plane

Here we list the numerical values of the special parameter points in the $\omega_{22} - r$ plane. For $Y_f^{(2)} = 0$, using the numerical values from eq. (2.18) for NO and putting them into eq. (2.32) we get:

$$Y_e^{(2)} = 0 \Rightarrow (r, \omega_{22}) = (0.558002, 1.21395), \tag{D.1}$$

$$Y_\mu^{(2)} = 0 \Rightarrow (r, \omega_{22}) = (-0.130718, 0.00977035), \tag{D.2}$$

$$Y_\tau^{(2)} = 0 \Rightarrow (r, \omega_{22}) = (0.155322, -0.0112205), \tag{D.3}$$

and for IO:

$$Y_e^{(2)} = 0 \Rightarrow (r, \omega_{22}) = (-0.973831, 0), \tag{D.4}$$

$$Y_\mu^{(2)} = 0 \Rightarrow (r, \omega_{22}) = (0.559934, -0.0992133), \tag{D.5}$$

$$Y_\tau^{(2)} = 0 \Rightarrow (r, \omega_{22}) = (0.617427, 0.0919401). \tag{D.6}$$

References

- [1] C. Athanassopoulos et al., *Results on $\nu_\mu \rightarrow \nu_e$ neutrino oscillations from LSND experiment*, *Phys. Rev. Lett.* **81** (1998) 1774–1777.
- [2] Y. Fukuda et al., *Evidence for oscillation of atmospheric neutrinos*, *Phys. Rev. Lett.* **81** (1998) 1562–1567.
- [3] K. Eguchi et al., *First results from KamLAND: Evidence for reactor anti-neutrino disappearance*, *Phys. Rev. Lett.* **90** (2003) 021802.
- [4] Q. R. Ahmad et al., *Direct evidence for neutrino flavor transformation from neutral current interactions in the Sudbury Neutrino Observatory*, *Phys. Rev. Lett.* **89** (2002) 011301.
- [5] A. Abada, C. Biggio, F. Bonnet, M. B. Gavela and T. Hambye, *Low energy effects of neutrino masses*, *JHEP* **12** (2007) 061, [[0707.4058](#)].
- [6] R. Coy and M. Frigerio, *Effective comparison of neutrino-mass models*, [2110.09126](#).
- [7] MEG collaboration, A. M. Baldini et al., *Search for lepton flavour violating muon decay mediated by a new light particle in the MEG experiment*, *Eur. Phys. J. C* **80** (2020) 858, [[2005.00339](#)].
- [8] BABAR collaboration, B. Aubert et al., *Searches for Lepton Flavor Violation in the Decays $\tau^\pm \rightarrow e^\pm \gamma$ and $\tau^\pm \rightarrow \mu^\pm \gamma$* , *Phys. Rev. Lett.* **104** (2010) 021802, [[0908.2381](#)].
- [9] K. Hayasaka et al., *Search for lepton flavor violating τ decays into three leptons with 719 million produced $\tau^+ \tau^-$ Pairs*, *Phys. Lett. B* **687** (2010) 139–143, [[1001.3221](#)].
- [10] SINDRUM collaboration, U. Bellgardt et al., *Search for the decay $\mu^+ \rightarrow e^+ e^+ e^-$* , *Nucl. Phys. B* **299** (1988) 1–6.
- [11] MEG II collaboration, A. M. Baldini et al., *The design of the MEG II experiment*, *Eur. Phys. J. C* **78** (2018) 380, [[1801.04688](#)].
- [12] BELLE-II collaboration, W. Altmannshofer et al., *The Belle II Physics Book*, *PTEP* **2019** (2019) 123C01, [[1808.10567](#)].
- [13] MU3E collaboration, A. Wasili, *The Mu3e Experiment Searching for the Lepton Flavour Violating Decay $\mu^+ \rightarrow e^+ e^+ e^-$* , *PoS ICHEP2020* (2021) 898.
- [14] COMET collaboration, R. Abramishvili et al., *COMET Phase-I Technical Design Report*, *PTEP* **2020** (2020) 033C01, [[1812.09018](#)].
- [15] V. Cirigliano, K. Fuyuto, C. Lee, E. Mereghetti and B. Yan, *Charged Lepton Flavor Violation at the EIC*, *JHEP* **03** (2021) 256, [[2102.06176](#)].
- [16] P. Minkowski, *$\mu \rightarrow e \gamma$ at a Rate of One Out of 10^9 Muon Decays?*, *Phys. Lett. B* **67** (1977) 421–428.
- [17] T. Yanagida, *Horizontal symmetry and masses of neutrinos*, in *Proceedings: Workshop on the Unified Theories and the Baryon Number in the Universe, Tsukuba, Japan, 13-14 Feb 1979*, vol. C7902131, pp. 95–99, 1979.
- [18] R. N. Mohapatra and G. Senjanovic, *Neutrino Mass and Spontaneous Parity Violation*, *Phys. Rev. Lett.* **44** (1980) 912.
- [19] A. Zee, *A Theory of Lepton Number Violation, Neutrino Majorana Mass, and Oscillation*, *Phys. Lett. B* **93** (1980) 389.

- [20] A. Pilaftsis, *Radiatively induced neutrino masses and large Higgs neutrino couplings in the standard model with Majorana fields*, *Z. Phys. C* **55** (1992) 275–282, [[hep-ph/9901206](#)].
- [21] E. Ma, *Verifiable radiative seesaw mechanism of neutrino mass and dark matter*, *Phys. Rev. D* **73** (2006) 077301, [[hep-ph/0601225](#)].
- [22] W. Grimus and H. Neufeld, *Radiative Neutrino Masses in an $SU(2) \times U(1)$ Model*, *Nucl. Phys. B* **325** (1989) 18–32.
- [23] S. Mandal, R. Srivastava and J. W. Valle, *The simplest scoto-seesaw model: Wimp dark matter phenomenology and higgs vacuum stability*, *Physics Letters B* **819** (2021) 136458.
- [24] S. Girmohanta, R. N. Mohapatra and R. Shrock, *Neutrino Masses and Mixing in Models with Large Extra Dimensions and Localized Fermions*, *Phys. Rev. D* **103** (2021) 015021, [[2011.01237](#)].
- [25] S. Girmohanta and R. Shrock, *Extra-dimensional model of dark matter*, *Phys. Rev. D* **104** (2021) 115021, [[2109.02670](#)].
- [26] G. Cacciapaglia and M. Rosenlyst, *Loop-generated neutrino masses in composite Higgs models*, *JHEP* **09** (2021) 167, [[2010.01437](#)].
- [27] M. Rosenlyst, *Technically natural Higgs boson from Planck scale*, *Phys. Rev. D* **106** (2022) 013002, [[2112.11588](#)].
- [28] D. Jurčiukonis and L. Lavoura, *Two-body lepton-flavour-violating decays in a 2HDM with soft family-lepton-number breaking*, *JHEP* **03** (2022) 106, [[2107.14207](#)].
- [29] N. G. Deshpande and E. Ma, *Pattern of symmetry breaking with two higgs doublets*, *Phys. Rev. D* **18** (Oct, 1978) 2574–2576.
- [30] T. Toma and A. Vicente, *Lepton Flavor Violation in the Scotogenic Model*, *JHEP* **01** (2014) 160, [[1312.2840](#)].
- [31] A. Vicente and C. E. Yaguna, *Probing the scotogenic model with lepton flavor violating processes*, *JHEP* **02** (2015) 144, [[1412.2545](#)].
- [32] N. Rojas, R. Srivastava and J. W. F. Valle, *Simplest Scoto-Seesaw Mechanism*, *Phys. Lett. B* **789** (2019) 132–136, [[1807.11447](#)].
- [33] S. Mandal, R. Srivastava and J. W. F. Valle, *The simplest scoto-seesaw model: WIMP dark matter phenomenology and Higgs vacuum stability*, *Phys. Lett. B* **819** (2021) 136458, [[2104.13401](#)].
- [34] D. N. Dinh, *The $\mu \rightarrow e\gamma$ decay in an EW-scale non-sterile RH neutrino model*, *Eur. Phys. J. C* **82** (2022) 295, [[2108.12613](#)].
- [35] J. Klarić, M. Shaposhnikov and I. Timiryasov, *Uniting Low-Scale Leptogenesis Mechanisms*, *Phys. Rev. Lett.* **127** (2021) 111802, [[2008.13771](#)].
- [36] R. W. Rasmussen and W. Winter, *Perspectives for tests of neutrino mass generation at the GeV scale: Experimental reach versus theoretical predictions*, *Phys. Rev. D* **94** (2016) 073004, [[1607.07880](#)].
- [37] K. Bondarenko, A. Boyarsky, D. Gorbunov and O. Ruchayskiy, *Phenomenology of GeV-scale Heavy Neutral Leptons*, *JHEP* **11** (2018) 032, [[1805.08567](#)].
- [38] M. Drewes, B. Garbrecht, D. Gueter and J. Klaric, *Testing the low scale seesaw and leptogenesis*, *JHEP* **08** (2017) 018, [[1609.09069](#)].

- [39] M.-C. Chen and J. Huang, *TeV Scale Models of Neutrino Masses and Their Phenomenology*, *Mod. Phys. Lett. A* **26** (2011) 1147–1167, [[1105.3188](#)].
- [40] J. Lopez-Pavon, E. Molinaro and S. T. Petcov, *Radiative Corrections to Light Neutrino Masses in Low Scale Type I Seesaw Scenarios and Neutrinoless Double Beta Decay*, *JHEP* **11** (2015) 030, [[1506.05296](#)].
- [41] D. N. Dinh and S. T. Petcov, *Lepton Flavor Violating τ Decays in TeV Scale Type I See-Saw and Higgs Triplet Models*, *JHEP* **09** (2013) 086, [[1308.4311](#)].
- [42] V. Dūdėnas and T. Gajdosik, *Low Seesaw Scale in the Grimus–Neufeld Model*, *Acta Phys. Polon. Supp.* **15** (2022) 1.
- [43] D. Fontes, M. Löschner, J. C. Romão and J. a. P. Silva, *Leaks of CP violation in the real two-Higgs-doublet model*, *Eur. Phys. J. C* **81** (2021) 541, [[2103.05002](#)].
- [44] J. A. Casas and A. Ibarra, *Oscillating neutrinos and $\mu \rightarrow e, \gamma$* , *Nucl. Phys. B* **618** (2001) 171–204, [[hep-ph/0103065](#)].
- [45] P. Athron, J.-h. Park, D. Stöckinger and A. Voigt, *FlexibleSUSY — A spectrum generator generator for supersymmetric models*, *Comput. Phys. Commun.* **190** (2015) 139–172, [[1406.2319](#)].
- [46] P. Athron, M. Bach, D. Harries, T. Kwasnitza, J.-h. Park, D. Stöckinger et al., *FlexibleSUSY 2.0: Extensions to investigate the phenomenology of SUSY and non-SUSY models*, *Comput. Phys. Commun.* **230** (2018) 145–217, [[1710.03760](#)].
- [47] P. Athron, A. Büchner, D. Harries, W. Kotlarski, D. Stöckinger and A. Voigt, *FlexibleDecay: An automated calculator of scalar decay widths*, [2106.05038](#).
- [48] H. E. Haber and G. L. Kane, *The Search for Supersymmetry: Probing Physics Beyond the Standard Model*, *Phys. Rept.* **117** (1985) 75–263.
- [49] PARTICLE DATA GROUP collaboration, P. Zyla et al., *Review of Particle Physics*, *PTEP* **2020** (2020) 083C01.
- [50] M. Reig, D. Restrepo, J. W. F. Valle and O. Zapata, *Bound-state dark matter with Majorana neutrinos*, *Phys. Lett. B* **790** (2019) 303–307, [[1806.09977](#)].
- [51] W. Grimus and L. Lavoura, *The Seesaw mechanism at arbitrary order: Disentangling the small scale from the large scale*, *JHEP* **11** (2000) 042, [[hep-ph/0008179](#)].
- [52] I. M. Ávila, G. Cottin and M. A. Díaz, *Revisiting the scotogenic model with scalar dark matter*, [2108.05103](#).
- [53] U. Khasianevich, W. Kotlarski and D. Stöckinger, *NPointFunctions: a calculator of amplitudes and observables in FlexibleSUSY*, in *Computational Tools for High Energy Physics and Cosmology*, 6, 2022. [2206.00745](#).
- [54] F. Staub, *Exploring new models in all detail with SARAH*, *Adv. High Energy Phys.* **2015** (2015) 840780, [[1503.04200](#)].
- [55] A. Vicente, *Computer tools in particle physics*, [1507.06349](#).
- [56] T. Hahn, *Generating Feynman diagrams and amplitudes with FeynArts 3*, *Comput. Phys. Commun.* **140** (2001) 418–431, [[hep-ph/0012260](#)].
- [57] T. Hahn and M. Perez-Victoria, *Automatized one loop calculations in four-dimensions and D-dimensions*, *Comput. Phys. Commun.* **118** (1999) 153–165, [[hep-ph/9807565](#)].

- [58] W. Kotlarski, D. Stöckinger and H. Stöckinger-Kim, *Low-energy lepton physics in the MRSSM: $(g-2)_\mu$, $\mu \rightarrow e\gamma$ and $\mu \rightarrow e$ conversion*, *JHEP* **08** (2019) 082, [[1902.06650](#)].
- [59] J. Hisano, T. Moroi, K. Tobe and M. Yamaguchi, *Lepton flavor violation via right-handed neutrino Yukawa couplings in supersymmetric standard model*, *Phys. Rev. D* **53** (1996) 2442–2459, [[hep-ph/9510309](#)].
- [60] Y. Okada, K.-i. Okumura and Y. Shimizu, *$\mu \rightarrow e\gamma$ and $\mu \rightarrow 3e$ processes with polarized muons and supersymmetric grand unified theories*, *Phys. Rev. D* **61** (2000) 094001, [[hep-ph/9906446](#)].
- [61] A. Crivellin, S. Davidson, G. M. Pruna and A. Signer, *Renormalisation-group improved analysis of $\mu \rightarrow e$ processes in a systematic effective-field-theory approach*, *JHEP* **05** (2017) 117, [[1702.03020](#)].
- [62] Y. Kuno and Y. Okada, *Muon decay and physics beyond the standard model*, *Rev. Mod. Phys.* **73** (2001) 151–202, [[hep-ph/9909265](#)].
- [63] A. Ilakovac and A. Pilaftsis, *Flavor violating charged lepton decays in seesaw-type models*, *Nucl. Phys. B* **437** (1995) 491, [[hep-ph/9403398](#)].
- [64] R. Kitano, M. Koike and Y. Okada, *Detailed calculation of lepton flavor violating muon electron conversion rate for various nuclei*, *Phys. Rev. D* **66** (2002) 096002, [[hep-ph/0203110](#)].
- [65] G. C. Branco, P. M. Ferreira, L. Lavoura, M. N. Rebelo, M. Sher and J. P. Silva, *Theory and phenomenology of two-Higgs-doublet models*, *Phys. Rept.* **516** (2012) 1–102, [[1106.0034](#)].
- [66] A. Arbey, F. Mahmoudi, O. Stal and T. Stefaniak, *Status of the Charged Higgs Boson in Two Higgs Doublet Models*, *Eur. Phys. J. C* **78** (2018) 182, [[1706.07414](#)].
- [67] R. Boto, T. V. Fernandes, H. E. Haber, J. C. Romão and J. a. P. Silva, *Basis-independent treatment of the complex 2HDM*, *Phys. Rev. D* **101** (2020) 055023, [[2001.01430](#)].
- [68] S. Davidson and H. E. Haber, *Basis-independent methods for the two-Higgs-doublet model*, *Phys. Rev. D* **72** (2005) 035004, [[hep-ph/0504050](#)].
- [69] H. E. Haber and D. O’Neil, *Basis-independent methods for the two-Higgs-doublet model. II. The Significance of $\tan\beta$* , *Phys. Rev. D* **74** (2006) 015018, [[hep-ph/0602242](#)].
- [70] H. E. Haber and D. O’Neil, *Basis-independent methods for the two-Higgs-doublet model III: The CP-conserving limit, custodial symmetry, and the oblique parameters S , T , U* , *Phys. Rev. D* **83** (2011) 055017, [[1011.6188](#)].
- [71] J. Kalinowski, W. Kotlarski, T. Robens, D. Sokolowska and A. F. Zarnecki, *Benchmarking the Inert Doublet Model for e^+e^- colliders*, *JHEP* **12** (2018) 081, [[1809.07712](#)].